Measurement of the state of polarisation of partially linear polarised infrared radiation by means of nematic liquid crystals

by
Pierre Drobniak (Matr. N°1428130)

Master's Thesis

for the degree of
Master of Science

submitted at
Vienna University of Technology

Tutor
Ao.Univ.-Prof. Dipl.-Ing. Dr.techn. Gerhard Liedl

Institute for Production Engineering and Laser Technology
Head: Univ.-Prof. Dipl-Ing. Dr.techn. Friedrich Bleicher

Faculty of Mechanical and Industrial Engineering

Vienna, November 2016

Table of Contents

1 Acknowledgement

First of all I would like to thank the people who directly worked with me. My Tutor Prof. Gerhard Liedl who was patient and always gave me his full authorisation and support on the ideas I had. Asst. Gerald Humenberger who dedicated a lot of his time to helping me throughout my project each time I encountered a difficulty. Manfred, the Technician (whose last name I never knew) who made the whole project possible by machining all the adapters and shafts necessary for the assembly.

I also would like to thank my co-worker Germán who helped me with his programming skills. Without him I would not have completed my Master's Thesis on time.

A last acknowledgement goes to my father who dared reading and correct my report, although his field of competance does not have anything to do with optics.

2 Introduction

2.1 Motivation for the project

Lasers are being increasingly used in the industrial world (Fig.2.1).

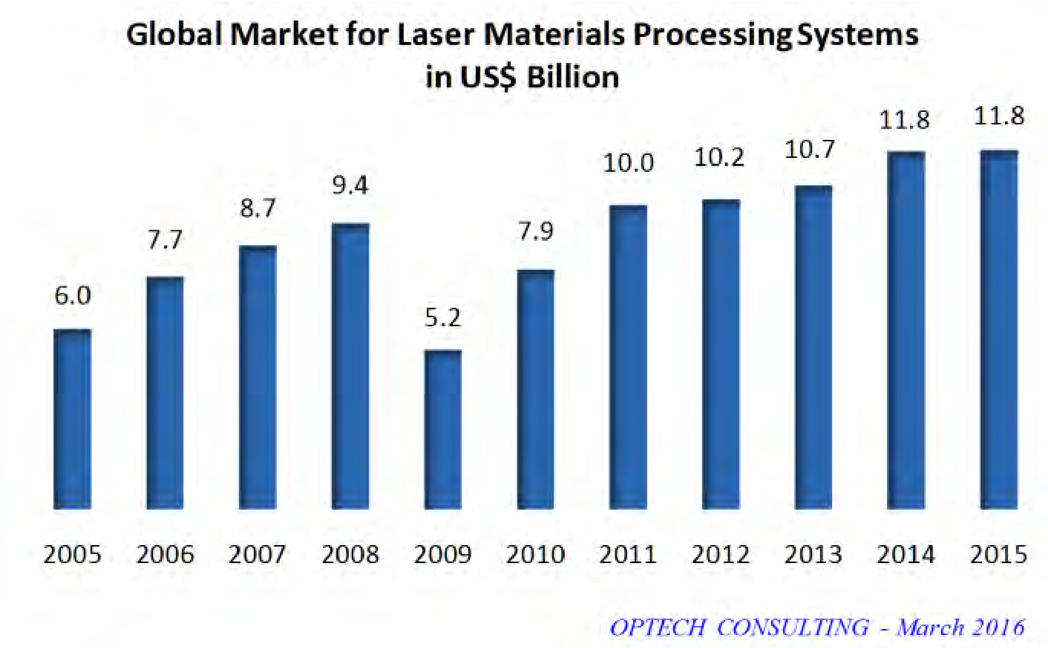

Figure 2.1: Global market for laser materials processing systems in US$ Billion

They are in fact very versatile tools, with a wide range of application such as bending [1], cutting [2], drilling [3], welding [4] or surface treatment [5] of materials. In order to monitor the performance of a laser process, it is necessary to measure the manufactured material quality.
A first way to proceed is to check the quality once the material is machined. This solution is relatively easy to implement, but does not give any informations about the process itself. As a matter of fact, it is quite difficult to relate measured characteristics of laser processed samples to process parameters. For example, in case of a laser drilled hole, one basic but effective way of determining hole shape and dimensions is to simply section the hole along its midplane [6]. However, this technique is intrusive and does not guarantee the quality of the next hole to be drilled.

Another course of action is the so called *in situ* measurement providing a quality assessment during the process. Some methods already exist, for example by means of X-Rays tomography (almost impossible to implement in an industrial process chain) or interferometry [6]. We will however try a new approach, using the laser machined material heating during the process and thus its infrared radiation.

When a material is being laser cut, the shape of the cut is slightly curved during the process (Fig.2.2).

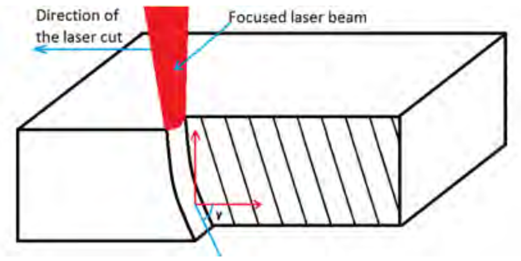

Figure 2.2: Laser cut material

In terms of quality control, we are interested in the determination of the angle γ. A similar problematic occurs when a material is being laser drilled (Fig.2.3).

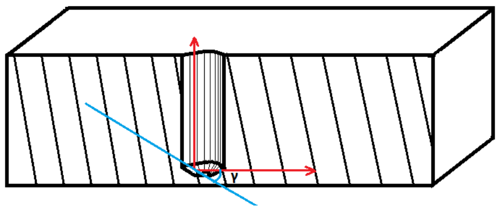

Figure 2.3: Sectional view of a laser drilled material

Here again, the bottom of the hole is curved. It would be interesting to measure the angle of curvature γ during the process.

Nowadays, automation of thermal material processing makes high demands on monitoring and controlling the resulting quality [7]. A new promising approach is the utilisation of emitted thermal radiation. The surface which is being laser machined is highly heated (around 1500°C). Theorised by Gustav Kirchhoff in 1862 and later on studied by Wilhelm Wien (Nobel Prize in Physics in 1911 for his discoveries on heat radiation laws), this heated body emits light due to thermal radiation [8]. The polarisation state of this emitted light depends on the angle of radiation [7] (Fig.2.4).

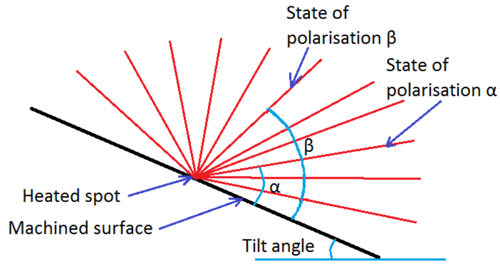

Figure 2.4: 2-D scheme of the radiated light on a spot of a heated surface

By measuring the state of polarisation of the radiated light for a given position of the set-up, we can then compute the angle γ.

The Master's Thesis topic will thus be the following: " Is it possible to derive the tilt angle of a laser heated surface using its infrared radiation? If so, how to build a fixed optical system, without any moving or rotating part, providing enough information for this purpose?".

2.2 Objective of the project

The first objective of the Master's Thesis is to build an optical setup including liquid crystals, which is able to measure the emission of an infrared radiating heated body. This assembly must yield enough informations to further compute the state of polarisation of a partially linear polarised infrared radiation. The system has to be fully electrically controlled, without any moving, or rotating part.
The second stage of the project is the testing of the optical setup on an infrared light source. For technical reasons, the latter will not be a laser heated radiating surface. An infrared emitter will be used instead. The generated polarisation states will be fully linear and all measurements in this project will be carried out on fully linear polarised light. Nevertheless, the system also works for partially linear polarised light.
A further objective would have been the testing of the assembly on a robot arm, while laser heating a surface. The objective would then have been to derive the tilt angle of this infrared radiating surface, thanks to the optical setup. Sadly, the granted time for this Master's Thesis does not permit to investigate this far on the subject. However, all informations for this purpose are given in section 6.2 and should be reused.

2.3 Distinctiveness of the project

The measurement of light polarisation by means of liquid crystals is not new and has already been investigated in 2002[9]. Nevertheless, the experiments in [9] where carried out using a HeNe laser while the light source in the following project is infrared and comes from a point source. This last detail makes the process more complicated than

with a parallel laser beam.
Another interesting paper on the subject [10] was published in 2010. However, in [10], a ferroelectric **smectic** C* liquid crystal device is used, whereas the LCVR (Liquid Crystal Variable Retarder) in this Master's Thesis is composed of **nematic** liquid crystals.
A recent publication [11] was made on the subject. In this paper, no special information is given about the wavelength of the measured polarised light. According to the specification of the utilised LCVR (LRC-200, Meadowlark Optics), the emission must have been between 450nm and 1800nm. In the following Master's Thesis, attention will be focused on infrared light emission around 1500nm.
Finally, what really makes the project different, new and interesting is the application of the optical system on a infrared radiating heated surface, in order to compute its tilt angle. The idea of using the state of polarisation of the radiation to compute the tilt angle is not new [7], but the combination with use of nematic liquid cystals is specific to this project.

3 Theoretical background

3.1 Basics of optics

3.1.1 Polarisation of light

Light is an electromagnetic transversal wave and thus can be described by the position of the electric vector in the plane normal to its direction of propagation (Fig.3.1).

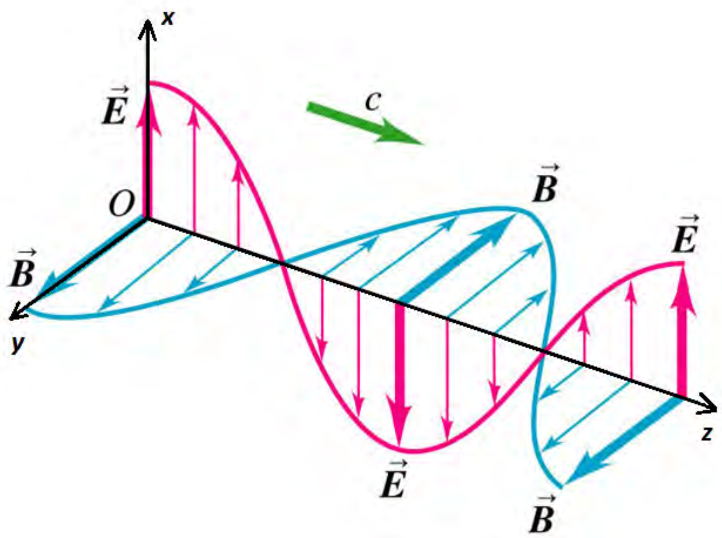

Figure 3.1: Propagation of a linear polarised electromagnetic field in z-direction [12]

The magnetic field can be neglected in comparison with the electric one. If we observe the motion in time of the electric field for a fixed value of z in the normal plane (perpendicular to the direction of propagation), we can observe several types of polarisation: linear, elliptic and circular polarisation (Fig.3.2).

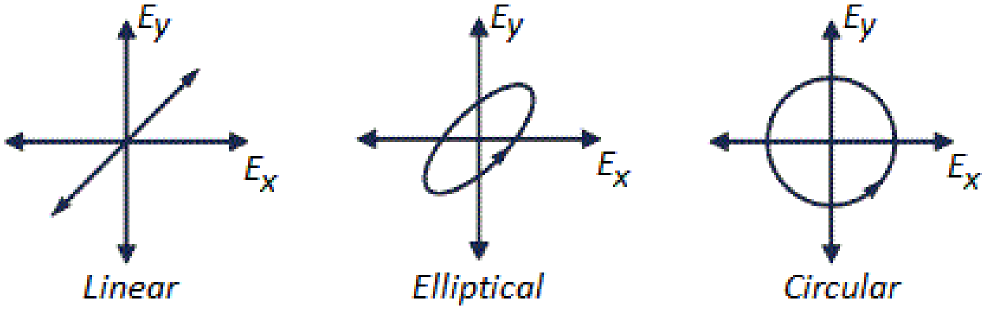

Figure 3.2: Three types of polarisation of light propagating in z-direction: (from left to right) linear, elliptic, circular

As described in Fig.3.2, it is more convenient to split the electric field in two orthogonal components E_x and E_y. The expression of the electric field at a time t and for a fixed value of z is then given by the following equation (3.1)[13]:

$$\vec{E}(z,t) = \begin{pmatrix} E_x(z,t) \\ E_y(z,t) \end{pmatrix} = \begin{pmatrix} E_{x0}\cos(\omega t - \frac{2\pi z}{\lambda} + \delta_x) \\ E_{y0}\cos(\omega t - \frac{2\pi z}{\lambda} + \delta_y) \end{pmatrix} \tag{3.1}$$

where E_x and E_y are the values of the electric field in the x- and y-direction at the position z and time t, E_{x_0} and E_{y_0} are the amplitudes of the x- and y-oscillations, δ_x and δ_y are the phases of the x- and y-oscillations at $z = 0$, ω is the angular frequency and λ is the wavelength.

With this formulation, any type of polarisation (linear, circular or elliptical) can thus be described by variation of the different values of δ_x and δ_y. Let us consider the position of the electric vector at $z = 0$. After some computation, we can get rid of the time component and thus write the following equation (3.2)[13]:

$$\frac{E_x^2}{E_{x_0}^2} + \frac{E_y^2}{E_{y_0}^2} - \frac{2E_xE_y\cos(\delta_y - \delta_x)}{E_{x_0}E_{y_0}} = \sin^2(\delta_y - \delta_x) \tag{3.2}$$

One recognizes in (3.2) the equation of an ellipse variating in the E_x-E_y-plane. The four parameters E_{x_0}, E_{y_0}, δ_x and δ_y are then enough to fully describe this ellipse. While it is possible to characterise the **shape** and **size** of the ellipse without any reference to a coordinate system, the orientation of the major axis (**azimuth**) as well as the rotation sense of the electric vector tip (**handedness**) must be referred to a fixed system.

The four values describing the ellipse are a (semi-major axis), b (semi-minor axis), ζ (azimuth) and the sign of $\delta_y - \delta_x$ (handedness). Let us introduce the ratio $\eta = b/a$ and the intensity of the beam $I = (a^2 + b^2)$. The equations ruling the parameters of the ellipse are then the following three (3.3), (3.4) and (3.5):

$$I = E_{x_0}^2 + E_{y_0}^2 \tag{3.3}$$

$$\tan(2\zeta) = \frac{2E_{x0}E_{y0}\cos(\delta_y - \delta_x)}{E_{x_0}^2 - E_{y_0}^2} \tag{3.4}$$

$$\frac{2\eta}{1+\eta^2} = \frac{2E_{x0}E_{y0}\cos(\delta_y - \delta_x)}{E_{x_0}^2 + E_{y_0}^2} \tag{3.5}$$

By solving this equations, we get the four parameters fully describing the ellipse: I, ζ , the numerical value of η and the sign of the deduced η.

The computation made earlier refers to fully polarised light. Nevertheless, light is always a combination of polarised and unpolarised light. Let us split these two parts, so that the full electric field would be a sum of a polarised and unpolarised component. The unpolarised component does not have a proper period and hence does not interfere with the polarised one. The full intensity I is then computed by (3.6):

$$I = I_u + I_p \tag{3.6}$$

where I_u represents the intensity of the unpolarised part and I_p the intensity of the polarised one.

We can then introduce the **degree of polarisation** p, which is defined as follows (3.7) [13][14]:

$$p = \frac{I_p}{I_u + I_p} \tag{3.7}$$

The degree of polarisation would get the value 1 for a fully polarised light beam and 0 for a fully unpolarised one.

3.1.2 Stokes parameters

After passing through a polariser, whose transmission axis is set at an angle α to the x-axis, the emergent intensity $I(\alpha)$ of a perfectly polarised light beam is given by (3.8) [13]:

$$I(\alpha) = E_{x_0}^2\cos^2(\alpha) + E_{y_0}^2\sin^2(\alpha) + E_{x0}E_{y0}\sin(2\alpha)\cos(\delta_y - \delta_x) \tag{3.8}$$

After some computation with the sine and cosine, we get the following equivalent harmonic equation (3.9) for the intensity:

$$I(\alpha) = A_0 + A_1\cos(2\alpha) + A_2\sin(2\alpha) \tag{3.9}$$

where $A_0 = \frac{1}{2}(E_{x_0}^2 + E_{y_0}^2)$, $A_1 = \frac{1}{2}(E_{x_0}^2 - E_{y_0}^2)$ and $A_2 = E_{x0}E_{y0}\cos(\delta_y - \delta_x)$.

Let us suppose that we carry out, beyond the polariser, three measurements of the intensity for three different angles. The results will yield us three of the four components required to fully describe the ellipse. The cosine function is indeed an even function and does not give us any information about the sign of $\delta_y - \delta_x$. We therefore need to perform an additional experiment by introducing a retarder ($\frac{\pi}{2}$ delay of one of the components of $\vec{E}$) before the polariser. The new intensity emerging from the polariser is then ${}_rI(\alpha)$ ruled by the following equation (3.10):

$$ {}_rI(\alpha) = {}_rA_0 + {}_rA_1\cos(2\alpha) + {}_rA_2\sin(2\alpha) \tag{3.10} $$

where ${}_rA_0 = \frac{1}{2}(E_{x_0}^2 + E_{y_0}^2) = A_0$, ${}_rA_1 = \frac{1}{2}(E_{x_0}^2 - E_{y_0}^2) = A_1$ and ${}_rA_2 = \pm E_{x_0}E_{y_0}\sin(\delta_y - \delta_x)$.

We choose the positive sign in the last equation, which means that the y-component is delayed by $\frac{\pi}{2}$ with respect to the x-component. This time, we got the handedness of the ellipse. However, it is not possible anymore to quantify the azimuth. Thus, for a **full description of the ellipse**, we need the values of A_0, A_1, A_2 and ${}_rA_2$. We can astutely notice that A_0 is only half of the full intensity of the light beam. It is then more convenient to work with four other constants called **Stokes parameters**. They are defined as follows (3.11):

$$ \begin{aligned} S_0 = I = Intensity \\ S_1 = 2A_1 \\ S_2 = 2A_2 \\ S_3 = 2{}_rA_2 \end{aligned} \tag{3.11} $$

We then define the Stokes vector $\vec{S}$ as (3.12):

$$ \vec{S} = \begin{pmatrix} S_0 \\ S_1 \\ S_2 \\ S_3 \end{pmatrix} \tag{3.12} $$

The first three parameters S_0, S_1 and S_2 can be rewritten in terms of simple intensity measurements performed with a linear polariser set to angles of 0°, 45° and 90° to the x-axis. Another expression for those parameters is then (3.13):

$$ \begin{aligned} S_0 = I(0°) + I(90°) \\ S_1 = I(0°) - I(90°) \\ S_2 = I(45°) - \frac{1}{2}(I(0°) + I(90°)) \end{aligned} \tag{3.13} $$

Actually, those three first Stokes parameters refer to linear polarised light. So, in case of light not containing any rotational (circular or elliptical) part, the value of S_3 is then 0.

Referring to the geometrical parameters of the ellipse, we obtain the following description given by Tab.3.1.

Size	S_0
Azimuth	$\frac{S_2}{S_1} = \tan(2\zeta)$
Shape	$\frac{\lvert S_3 \rvert}{S_0} = \frac{2\eta}{1+\eta^2}$
Handedness	Sign of S_3

Table 3.1: Full description of the ellipse with the Stokes parameters

Now that we have defined the Stokes parameters, it is then possible to introduce the degree of polarisation p as a function of S_0, S_1, S_2 and S_3 (3.14) :

$$p = \frac{I_p}{I_u + I_p} = \frac{(S_1^2 + S_2^2 + S_3^2)^{\frac{1}{2}}}{I_u + I_p} = \frac{(S_1^2 + S_2^2 + S_3^2)^{\frac{1}{2}}}{S_0} \tag{3.14}$$

where I_u and I_p refer respectively to the intensity of the unpolarised and polarised part of the light beam.

Tab.3.2 sums up particular Stokes vectors, each of whom corresponding to a different polarisation state [14].

Polarisation State	Stokes Vector
horizontal linear state	$\begin{pmatrix}1\\1\\0\\0\end{pmatrix}$
vertical linear state	$\begin{pmatrix}1\\-1\\0\\0\end{pmatrix}$
linear state at $+45°$	$\begin{pmatrix}1\\0\\1\\0\end{pmatrix}$
linear state at $-45°$	$\begin{pmatrix}1\\0\\-1\\0\end{pmatrix}$
right-handed circular state	$\begin{pmatrix}1\\0\\0\\1\end{pmatrix}$
left-handed circular state	$\begin{pmatrix}1\\0\\0\\-1\end{pmatrix}$

Table 3.2: Stokes vectors for particular states of polarisation

One must notice that the values presented in Tab.3.2 are normalized so that the full intensity I is equal to 1. One can also note that for **linear** polarised light, the last component of the Stokes vector is equal to 0. In that case, it is more convenient to work with shortened Stokes vectors containing only three components.

3.1.3 Mueller matrices

Let us consider an incident partially polarised light beam, described by its Stokes vector $\vec{S_i}$, which passes through an optical system. The output vector $\vec{S_t}$ is then the input vector $\vec{S_i}$ modified by the optical element. This physical process can be mathematically described by a 4×4 matrix $\mathbf{A}$. This matrix $\mathbf{A}$ is called the **Mueller matrix** of the optical system. Thus we can then get the following relation (3.15)[14]:

$$\vec{S_t} = \mathbf{A}\vec{S_i} \tag{3.15}$$

where $\mathbf{A} = \begin{pmatrix} a_{11} & a_{12} & a_{13} & a_{14} \\ a_{21} & a_{22} & a_{23} & a_{24} \\ a_{31} & a_{32} & a_{33} & a_{34} \\ a_{41} & a_{42} & a_{43} & a_{44} \end{pmatrix}$, $\vec{S_t} = \begin{pmatrix} S_{t,0} \\ S_{t,1} \\ S_{t,2} \\ S_{t,4} \end{pmatrix}$ and $\vec{S_i} = \begin{pmatrix} S_{i,0} \\ S_{i,1} \\ S_{i,2} \\ S_{i,4} \end{pmatrix}$.

This result can be rewritten in (3.16) as a system of 4 equations:

$$\begin{aligned} S_{t0} &= a_{11}S_{i,0} + a_{12}S_{i,1} + a_{13}S_{i,2} + a_{14}S_{i,3} \\ S_{t1} &= a_{21}S_{i,0} + a_{22}S_{i,1} + a_{23}S_{i,2} + a_{24}S_{i,3} \\ S_{t2} &= a_{31}S_{i,0} + a_{32}S_{i,1} + a_{33}S_{i,2} + a_{34}S_{i,3} \\ S_{t3} &= a_{41}S_{i,0} + a_{42}S_{i,1} + a_{43}S_{i,2} + a_{44}S_{i,3} \end{aligned} \tag{3.16}$$

Tab.3.3 lists the Mueller matrices of some particular optical devices [15]. The latter are ideal, which means that the degree of transmission is 100%. Let us give some explanation on the working principle of the optical components given in Tab.3.3:

- A linear polariser transforms a non linear incident light beam into a linear one. The plane of polarisation of the outgoing linearly polarised light is then defined by the angle of the linear polariser with a fixed reference.
- A wave plate is an optical device possessing two orthogonal axis, called respectively slow- and fast-axis. In order to understand its working principle, let us split the incident light beam in two components, respectively one on the fast- and another on the slow-axis. The component induces a phase shift between slow- and fast-axis. Depending on the phase shift, several behaviours occur:
  1. A quarter-wave plate induces a 90° phase shift between slow- and fast-axis (quarter means a spatial phase shift of one fourth of the wavelength). One can notice that a quarter-wave plate changes a linearly polarised incident light beam into a circular/elliptical one. The choice between circular and elliptical depends on the orientation of the incident light beam with the slow(or fast)-axis of the quarter-wave plate. For the particular case of an incident linear polarisation at an angle of 45° with the slow/fast-axis, the outgoing light beam will be circularly polarised.
  2. A half-wave plate has the same working principle as a quarter-wave plate, but induces a 180° phase shift between slow- and fast-axis.
- Variable retarders provide a variable phase shift. They can also be used as quarter- or half-wave plates.

Another advantage of Mueller formalism is the fact that the combination of several components can be described by simply multiplying the Mueller matrices of each components. Nevertheless, attention has to be paid on the order of appearance of the matrices. The matrix of the first component that the light beam meets is the first one to multiply the incident vector, then comes the second one, and so on. An example is given in the following equation (3.17) where a light beam first meets an optical component with the Mueller matrix $\mathbf{A}$ and then a second one described by $\mathbf{B}$:

$$\vec{S_t} = \mathbf{B}\mathbf{A}\vec{S_i} \tag{3.17}$$

Optical Element	Mueller Matrix
Ideal linear polariser	$\frac{1}{2}\begin{pmatrix} 1 & C & S & 0 \\ C & C^2 & CS & 0 \\ S & CS & S^2 & 0 \\ 0 & 0 & 0 & 0 \end{pmatrix}$
Ideal quarter-wave plate	$\begin{pmatrix} 1 & 0 & 0 & 0 \\ 0 & C^2 & SC & -S \\ 0 & SC & S^2 & C \\ 0 & S & -C & 0 \end{pmatrix}$
Ideal half-wave plate	$\begin{pmatrix} 1 & 0 & 0 & 0 \\ 0 & C^2 - S^2 & 2SC & 0 \\ 0 & -2SC & S^2 - C^2 & 0 \\ 0 & 0 & 0 & -1 \end{pmatrix}$
Ideal variable retarder	$\begin{pmatrix} 1 & 0 & 0 & 0 \\ 0 & C^2 + S^2\cos(\delta) & SC(1-\cos(\delta)) & -S\sin(\delta) \\ 0 & SC(1-\cos(\delta)) & S^2 + C^2\cos(\delta) & C\sin(\delta) \\ 0 & S\sin(\delta) & -C\sin(\delta) & \cos(\delta) \end{pmatrix}$

where $C = \cos(2\alpha)$, $S = \sin(2\alpha)$, α is the angle between the axis of the polariser (in case of a linear polariser) or the fast-axis (in case of a wave plate or a variable retarder) and a fixed reference (the horizon for example), δ is the phase shift introduced by the variable retarder.

Table 3.3: Mueller matrices of optical components for different configurations

3.2 Determination of an unknown linear Stokes vector

In this part, the aim is to compute the value of an unknown partially linear polarised Stokes vector for a given Mueller matrix of an electrically controlled optical system.

Let us consider an optical setup composed of different optical components, with at least one electro-optical device (a LCVR for example). The whole system can be described by its Muller matrix $\mathbf{M}$ (3.18):

$$\mathbf{M}(V) = \begin{pmatrix} a_{11}(V) & a_{12}(V) & a_{13}(V) & a_{14}(V) \\ a_{21}(V) & a_{22}(V) & a_{23}(V) & a_{24}(V) \\ a_{31}(V) & a_{32}(V) & a_{33}(V) & a_{34}(V) \\ a_{41}(V) & a_{42}(V) & a_{43}(V) & a_{44}(V) \end{pmatrix} \tag{3.18}$$

One can notice that $\mathbf{M}$ depends on the voltage V. Indeed, the variation of the voltage V applied on the electro-optical device makes the whole behaviour of the setup vary, and thus changes its Mueller matrix. This condition is important, since it allows us to proceed to different measurements, by only varying the voltage.

Let us then take an unknown incident partially linear poarlised Stokes vector $\vec{S_{in}}$ (3.19):

$$\vec{S_{in}} = \begin{pmatrix} S_{in,0} \\ S_{in,1} \\ S_{in,2} \\ 0 \end{pmatrix} \tag{3.19}$$

After its passage through the optical system, $\vec{S_{in}}$ becomes $\vec{S_{out}}$ and the following relation can be written (3.20):

$$\vec{S_{out}} = \begin{pmatrix} S_{out,0} \\ S_{out,1} \\ S_{out,2} \\ S_{out,3} \end{pmatrix} = \mathbf{M} \times \vec{S_{in}} = \begin{pmatrix} a_{11}(V)S_{in,0} + a_{12}(V)S_{in,1} + a_{13}(V)S_{in,2} \\ a_{21}(V)S_{in,0} + a_{22}(V)S_{in,1} + a_{23}(V)S_{in,2} \\ a_{31}(V)S_{in,0} + a_{32}(V)S_{in,1} + a_{33}(V)S_{in,2} \\ a_{41}(V)S_{in,0} + a_{42}(V)S_{in,1} + a_{43}(V)S_{in,2} \end{pmatrix} \tag{3.20}$$

When we measure the output intensity, we only get access to the value of $S_{out,0}$. So let us rewrite the first line of equation (3.20) in (3.21):

$$S_{out,0} = a_{11}(V)S_{in,0} + a_{12}(V)S_{in,1} + a_{13}(V)S_{in,2} \tag{3.21}$$

If we consider that the values of $a_{1j}(V)$ $(j = 1, 2, 3)$ are known and that the output intensity S_{out} can be measured, the equation (3.21) has three unknowns: $S_{in,0}$, $S_{in,1}$ and $S_{in,2}$. This mathematically means that we need two other equations, obtained for two other voltages applied to the LCVR. Let us thus call the three voltages V_1, V_2 and V_3. After measuring the output intensity for V_1, V_2 and V_3 we get the following system of equations (3.22):

$$
\begin{aligned}
S_{out,0}(V_1) &= a_{11}(V_1)S_{in,0} + a_{12}(V_1)S_{in,1} + a_{13}(V_1)S_{in,2} \\
S_{out,0}(V_2) &= a_{11}(V_2)S_{in,0} + a_{12}(V_2)S_{in,1} + a_{13}(V_2)S_{in,2} \\
S_{out,0}(V_3) &= a_{11}(V_3)S_{in,0} + a_{12}(V_3)S_{in,1} + a_{13}(V_3)S_{in,2}
\end{aligned} \tag{3.22}
$$

Let us build a vector $\vec{I}(V_1, V_2, V_3)$ containing the values of the three measured output intensities. The system of equations (3.22) can be rewritten as follows (3.23):

$$
\vec{I}(V_1, V_2, V_3) = \begin{pmatrix} S_{out,0}(V_1) \\ S_{out,0}(V_2) \\ S_{out,0}(V_3) \end{pmatrix} = \mathbf{A}(V_1, V_2, V_3) \times \begin{pmatrix} S_{in,0} \\ S_{in,1} \\ S_{in,2} \end{pmatrix} \tag{3.23}
$$

where $\mathbf{A}(V_1, V_2, V_3) = \begin{pmatrix} a_{11}(V_1) & a_{12}(V_1) & a_{13}(V_1) \\ a_{11}(V_2) & a_{12}(V_2) & a_{13}(V_2) \\ a_{11}(V_3) & a_{12}(V_3) & a_{13}(V_3) \end{pmatrix}$.

First case scenario: the matrix $\mathbf{A}(V_1, V_2, V_3)$ is invertible. Then the unknown incident partially linear Stokes vector $\vec{S_{in}}$ components ($S_{in,0}$, $S_{in,1}$ and $S_{in,2}$) are found by inverting $\mathbf{A}(V_1, V_2, V_3)$ (3.24):

$$
\begin{pmatrix} S_{in,0} \\ S_{in,1} \\ S_{in,2} \end{pmatrix} = \mathbf{A}^{-1} \times \vec{I}(V_1, V_2, V_3) \tag{3.24}
$$

This case would be perfect, for it would provide a quick way to get the incident state of polarisation. Nevertheless, one must bear in mind that inverting the matrix $\mathbf{A}$ physically means that the optical setup provides enough informations on the unknown incident Stokes vector $\vec{S_{in}}$, in order to derive the latter. Since $\vec{S_{in}}$ is partially polarised, and the setup only has influence on its polarised part, it is necessary to somehow get either the value of the full intensity $S_{in,0}$ of $\vec{S_{in}}$ or the degree of polarisation of $\vec{S_{in}}$. This means that a certain configuration of the optical setup has to provide the value of the full intensity $S_{in,0}$. If not, the matrix $\mathbf{A}$ is not invertible, and the full intensity $S_{in,0}$ (or the state of polarisation) has to be externally measured.

Second case scenario: the matrix $\mathbf{A}(V_1, V_2, V_3)$ is not invertible. And actually, due to the optical behaviour of the setup used in our project (LCVR+Analyser), the matrix $\mathbf{A}$ is non invertible. A mathematical explanation for this is given in section 4.2.

We then have to find another way to compute the values $S_{in,0}$, $S_{in,1}$ and $S_{in,2}$. Two solutions are then possible:

- either measure the full intensity of $\vec{S_{in}}$ or
- know its degree of polarisation.

The first solution is based on the fact that the first coefficient $S_{in,0}$ describes the full intensity of the incident light beam. By measuring separately the incident intensity $S_{in,0}$, only two unknowns remain: $S_{in,1}$ and $S_{in,2}$. In order to determine those two unknowns, we only need two equations, which means proceeding to two different measurements of the output intensity for two different voltages (V_1 and V_2). We then get the following relation (3.25):

$$\begin{aligned} S_{out,0}(V_1) &= a_{11}(V_1)S_{in,0} + a_{12}(V_1)S_{in,1} + a_{13}(V_1)S_{in,2} \\ S_{out,0}(V_2) &= a_{11}(V_2)S_{in,0} + a_{12}(V_2)S_{in,1} + a_{13}(V_2)S_{in,2} \end{aligned} \tag{3.25}$$

The difference with (3.22) is that we now only have two unknowns ($S_{in,1}$ and $S_{in,2}$) for two equations. If we shift the terms linked to $S_{in,0}$ to the left side and write the system in terms of matrices, we get (3.26):

$$\vec{J}(V_1, V_2) = \begin{pmatrix} S_{out,0}(V_1) - a_{11}(V_1)S_{in,0} \\ S_{out,0}(V_2) - a_{11}(V_2)S_{in,0} \end{pmatrix} = \mathbf{B}(V_1, V_2) \times \begin{pmatrix} S_{in,1} \\ S_{in,2} \end{pmatrix} \tag{3.26}$$

where $\mathbf{B}(V_1, V_2) = \begin{pmatrix} a_{12}(V_1) & a_{13}(V_1) \\ a_{12}(V_2) & a_{13}(V_2) \end{pmatrix}$.

By inverting the matrix $\mathbf{B}$, the values of $S_{in,1}$ and $S_{in,2}$ are computed, as shown in (3.27):

$$\begin{pmatrix} S_{in,1} \\ S_{in,2} \end{pmatrix} = \mathbf{B}^{-1} \times \vec{J}(V_1, V_2) \tag{3.27}$$

One question remains: is $\mathbf{B}$ invertible? It will be mathematically proven in section 4.2 that the matrix $\mathbf{B}$ of the setup used in our project is invertible.
The incident Stokes vector $\vec{S_{in}}$ can thus be reconstructed with $S_{in,0}$, $S_{in,1}$ and $S_{in,2}$.

The second way of proceeding is to get access to the degree of polarisation of the unknown incident light beam. Thanks to equation (3.14), $S_{in,0}$ can be rewritten in terms of $S_{in,1}$, $S_{in,2}$ and the degree of polarisation p. We then only have two unknowns to be derived. The system of equations to be solved can be written as follows (3.28):

$$\begin{aligned} S_{out,0}(V_1) &= a_{11}(V_1)\frac{1}{p}\sqrt{S_{in,1}^2 + S_{in,2}^2} + a_{12}(V_1)S_{in,1} + a_{13}(V_1)S_{in,2} \\ S_{out,0}(V_2) &= a_{11}(V_2)\frac{1}{p}\sqrt{S_{in,1}^2 + S_{in,2}^2} + a_{12}(V_2)S_{in,1} + a_{13}(V_2)S_{in,2} \end{aligned} \tag{3.28}$$

In the case where we know the value of p, the system (3.28) is mathematically solvable. And for a fully polarised incident light, this method is easy to implement, because p is then equal to 1 and thus does not need to be externally measured.

3.3 Working principle of liquid crystals

Nowadays, liquid crystals have a wide range of application. They are mostly famous for being used in LCD-screens but also play an increasing role in medicine [16]. In this section 3.3, we will only deal with a specific type of liquid crystals called **nematic**. The latter are composed of molecules whose orientation influence the polarisation of light passing through. This liquid is then confined between two polymer layers and two glass walls [17]. An example is shown in Fig.3.3.

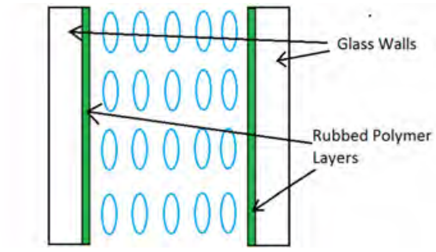

Figure 3.3: Homeotropic alignment of a nematic liquid crystal cell

A way to create homeotropic alignment is to treat the cell walls with a surfactant such as hexadecyl-trimethyl ammoniumbromide (HTAB) [18]. Due to the alignment of the molecules and their optical activity, the medium is then anisotropic. In fact, it is birefringent and allows us to define two main axis of refraction: one slow- and one fast-axis [17]. By applying an electric field between the two confining surfaces, it is then possible to influence the orientation of the molecules in the cell and thus control the birefringence of the medium [17] (Fig.3.4).

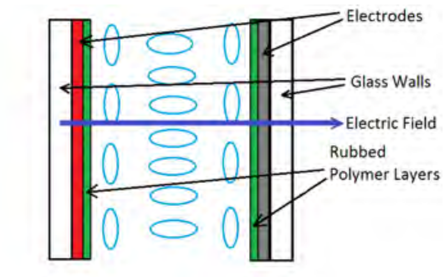

Figure 3.4: Influence of an electric field on the alignment of the molecules in a nematic liquid crystal cell

Let us consider an incident polarised light beam $\vec{E}_i$. The transmitted light is denoted $\vec{E}_t$. After its passage through the liquid crystal cell, the x- and y-components of the incident beam will undergo a phase shift. The transmitted polarisation state is then different from the incident one. The process is decribed in Fig.3.5.

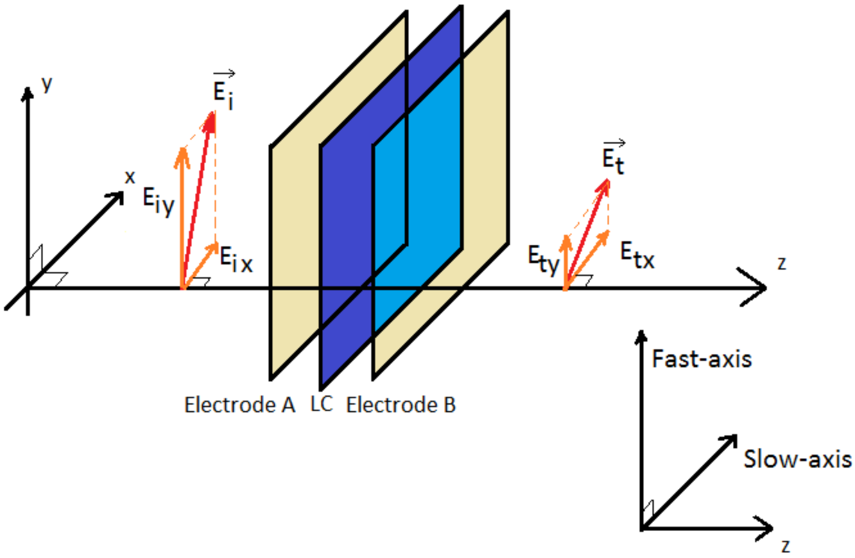

Figure 3.5: Phase shift caused by a liquid crystal cell between the two components of a polarised light beam

Another more accurate way to describe the liquid crystal cell is to write its Mueller matrix. As explained above, the liquid crystal cell induces a phase shift between the two components of the incident polarised light beam. This phase shift depends on the relative orientation of the incident light beam polarisation vector with slow- and fast-axis of the crystal. According to Mueller formalism, the Mueller matrix of a liquid crystal variable retarder $\mathbf{R}$, with retardation δ and fast-axis azimuthal angle α can be written as (3.29)[19]:

$$\mathbf{R} = \begin{pmatrix} 1 & 0 & 0 & 0 \\ 0 & C^2 + S^2 \cos(\delta(V)) & SC(1 - \cos(\delta(V))) & -S\sin(\delta(V)) \\ 0 & SC(1 - \cos(\delta(V))) & C^2 + S^2 \cos(\delta(V)) & C\sin(\delta(V)) \\ 0 & S\sin(\delta(V)) & -C\sin(\delta(V)) & \cos(\delta(V)) \end{pmatrix} \tag{3.29}$$

where $C = \cos(2\alpha)$, $S = \sin(2\alpha)$ and V is the RMS voltage applied between the electrodes.

The equation (3.29) is an ideal case where the liquid crystal cell has a perfect transmission (no loss of intensity). It is important to notice that the phase shift δ is a function of V, where V represents the RMS (Root Mean Square) value of the voltage. Indeed, the LCVR has to be driven by an **alternating** voltage of several kHz and without offset, in order to avoid the build-up of residual charges on its walls, which may damage the component.

3.4 Polarised thermal radiation

3.4.1 P- and S-polarisation

As a prerequisite to understanding the state of polarisation contained in a radiating heated surface, one must introduce the concept of p- and s-polarisation. A good way to visualise it is to picture an incident light beam on a reflecting surface (Fig.3.6).

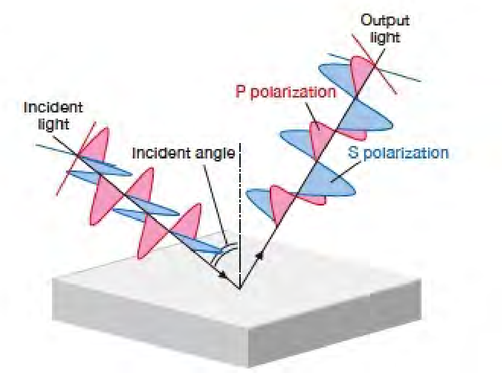

Figure 3.6: P- and s-polarisation of a reflected light beam [20]

The polarisation of the incident and the outgoing light beam is divided in two components. The s-polarisation is parallel to the plane defined by the reflecting surface. The p-component is then contained in the plane of incidence. This principle can be reused in case of a partially linear polarised radiated light, where the latter corresponds to the output light drawn in Fig.3.6.

3.4.2 Spectral radiation of a heated body

The spectral radiation density of a black body $L_{\lambda,B}(\lambda, T)$ at temperature T and wavelength λ can be described by Planck's law [21]. However, a black body describes the **ideal** behaviour of a heated radiating body, which cannot be achieved by a normal surface. The relationship between the radiation density of a real surface $L_\lambda(\lambda, T, \beta,$ *surface conditions, material*) and a black body can be expressed by the spectral emissivity $\boldsymbol{\epsilon}$ [7]. This emissivity is a function of the wavelength λ, the temperature T, the surface conditions such as roughness and oxidation and also of the used material. Additionally, the emissivity of a real surface is defined by the angle of radiation β and the state of polarisation (p- and s-polarisation)[7]. The relation between state of polarisation and angle of emission is described in Fig.3.7[7] for a piece of steel emitting at 1060 nm.

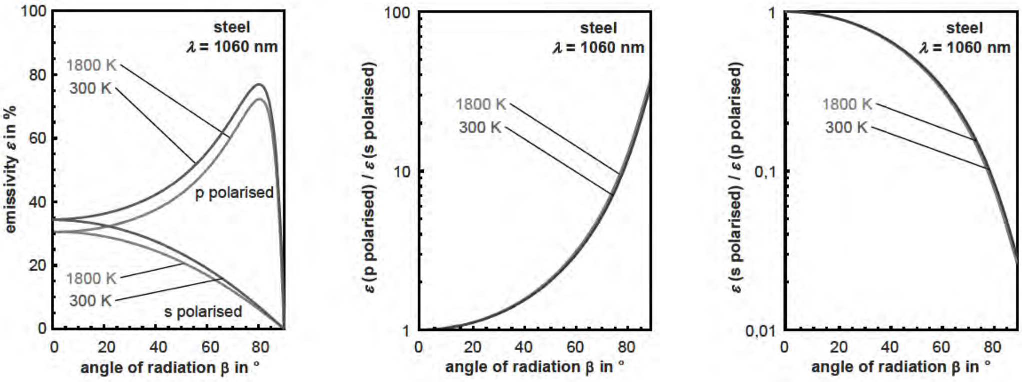

Figure 3.7: (a) Influence of the angle of radiation β and polarisation state on the emissivity ϵ at room (300K) and melting (1800K) temperature; (b) p- over s-polarisation emissivity ratio as a function of the angle of radiation β; (c) s-over p-polarisation emissivity ratio as a function of the angle of radiation β [7].

In Fig.3.7(c), one can notice that the ratio between the emissivity of s- over p-polarisation is a clear function of the angle of radiation. By computing the ratio $\frac{\epsilon(\text{s-polarised})}{\epsilon(\text{p-polarised})}$, it is then possible to get the angle of radiation β and thus the value of the angle γ, as defined in section 2.1. Theoretically, the thermal radiation gives us enough informations in order to quantify the quality of the investigated laser process.

4 Description of the setup

4.1 Physical description of the optical setup

The optical assembly used in this Master's Thesis is composed of several optical and electro-optical devices. A scheme is given in Fig.4.1 and a picture of the whole setup in Fig.4.2.

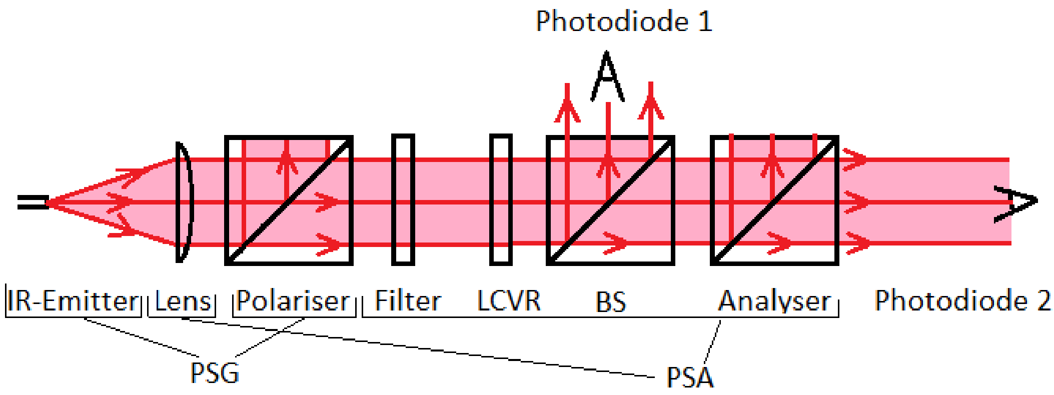

Figure 4.1: Scheme of the electro-optical assembly

Figure 4.2: Picture of the electro-optical assembly

The setup can be divided in two main parts: the **polarisation state generator** (**PSG**) and the **polarisation state analyser** (**PSA**). The PSG is composed of an infrared emitter (IR-emitter) and a polariser. Its role is to simulate the linear polarisation required for the experiments. The PSA allows for the generated linear polarisation examination.

In a further phase, where the setup would be tested in situ, the PSG would be removed and the optical assembly would only be composed of the PSA. In Fig.4.1, a gap can be seen between the lens and the filter. In order to make the system more compact, the lens can simply be shifted to the right, for its relative position to the optical assembly is not important. Only its position to the source matters.

The first PSG component is the infrared emitter (IR-Si295, Hawk Eye Technologies). It generates an infrared radiation from visible light to several μm. The technical data (Fig.4.3) given by the manufacturer only starts at 2μm, nevertheless, the emitter still radiates light in the range of 1500nm. This fact is easily proven in section 5, since the photodiode receives a signal once the radiation is filtered around 1500nm.

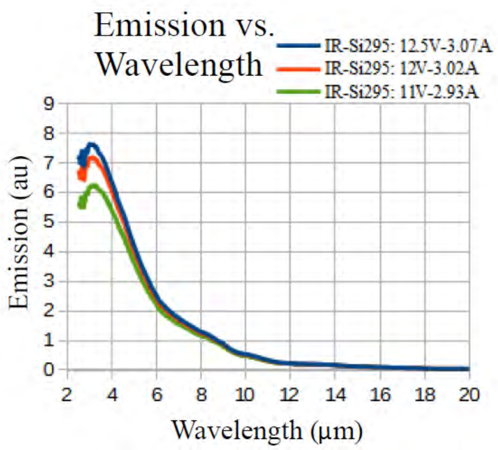

Figure 4.3: Emission spectrum of the IR-Si295 (Hawkeye Technologies datasheet)

A picture of the component is given in Fig.4.4.

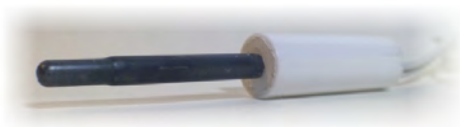

Figure 4.4: IR-Si295 Emitter (Hawkeye Technologies datasheet)

The emitter is heated around 1000°C and thus radiates light. The latter should be partially linear polarised, since it is coming from a heated surface (section 3.4). Nevertheless, the point where the setup is focused coincides with the tip of the emitter. At this particular point, one can make the approximation, that the radiated light is non-polarised. Actually, the light is slightly polarised, but this detail is not important, since all measurements in this Master's Thesis are carried out after a linear polariser, and thus with fully linear polarised light.

The first component that the light meets is the lens (LA4306, Thorlabs Inc). Informations concerning its dimensions are presented in Fig.4.5.

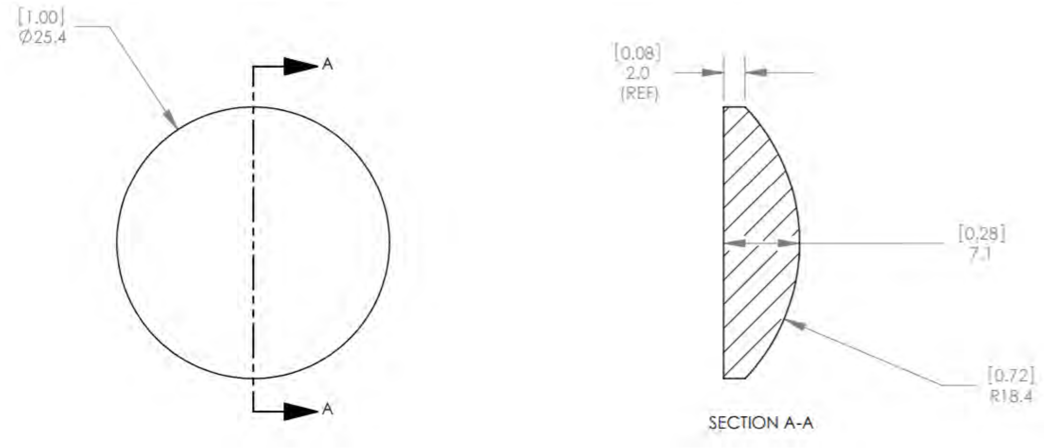

Figure 4.5: Dimensions of the LA4306 lens (Thorlabs datasheet)

Its focal length for 1500nm can be approximated around 70mm. The derivation of the latter is detailed in section 5.1 since the only informations provided by the manufacturer are valid between 250nm and 400nm and the refractive index of the lens depends on the wavelength [22]. The role of this component is the focus of all light rays emerging from the tip of the IR-emitter. Thus, all light rays arising from the focal point are parallel after the lens and hence the intensity does not decrease along its optical path in the optical setup. The use of a lens has two major advantages:

- the intensity measured by the photodiode is higher than without lens
- the difference of the measured intensity between photodiode 1 and 2 only depends on the effect of the components along each optical path.

This second point is a major issue, since the whole computation of the unknown state of polarisation is based on the optical components impact on the measured intensity. If the light rays were not parallel, it would be difficult (not impossible) to know which part of the intensity difference between photodiode 1 and 2 arises from the beam divergence and which part comes from the optical devices. A simple solution to get rid of the influence of the beam divergence would have been the elaboration of a setup where the optical paths from the source to photodiode 1 and 2 (now called optical paths 1 and 2) have the same length. Those two optical paths are detailed in Fig.4.6.

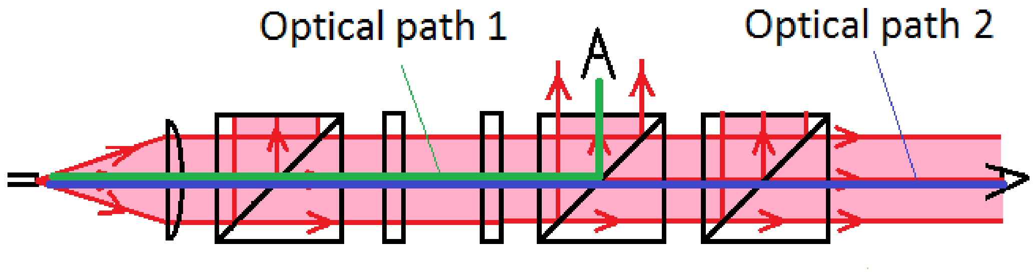

Figure 4.6: Optical paths 1 and 2

Nevertheless, for technical reasons, the optical paths 1 and 2 do not have the same length. Indeed, in the beam-splitter (BS in Fig.4.1), the light beam is separated in two components with a right angle. In order to avoid a too long lever arm on the beam-splitter, the optical path between beam-splitter and photodiode 1 is as short as possible. Sadly, due to the presence of the analyser after the beam-splitter, the optical path 2 is longer and cannot be shortened.
As mentionned in the previous lines, it is not impossible to work without lens. Nevertheless, even if the difference of distance in the optical paths 1 and 2 is known, the loss of intensity due to the divergence needs a third external measurement of the absolute distance to the source. As a matter of fact, one can imagine that the intensity loss due to the divergence between optical paths 1 and 2 is not the same for a very close source (high divergence) as for a far away one (low divergence).
If the experiment were carried out with a laser beam, no lens would have been required and the experiment would have been easier to implement. Nevertheless, in case of a radiating heated surface during a laser machining process, the point source radiates light in all directions.

The light beam then travels through the second PSG component: the polariser. For technical reasons, the latter is actually a polarising beam-splitter (CCM1-PBS254/M, Thorlabs Inc) with a 50:50 splitting behaviour. Only one of its output is used and yields a linear polarised outgoing light beam, with a 50% loss due to the second unused output. A picture is given in section 4.7.

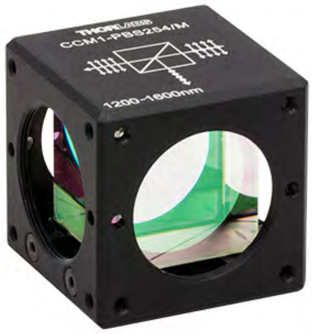

Figure 4.7: CCM1-PBS254/M Polarising beam-splitter [23]

Its behaviour is introduced in Fig.4.8.

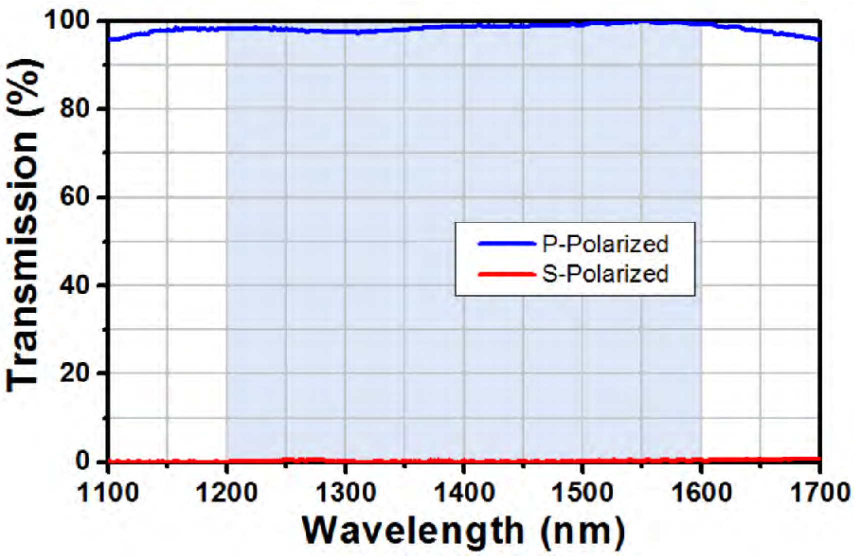

Figure 4.8: Splitting behaviour of the CCM1-PBS254/M beam-splitter [24]

The blue curve in Fig.4.8 shows the splitting behaviour on one output of the beam-splitter. This means that, for a P-polarised incident light, the output having the exact same orientation angle as the P-polarisation will yield an outgoing light with a the same P-polarisation and with a transmission coefficient of 100% in case of a 1500nm wavelength.

The next component is a filter (bk-1500-090-B, Interferenzoptik Elektronik GmbH). A picture can be found in Fig.4.9.

Figure 4.9: Picture of the bk-1500-090-B bandpass filter

Actually, it could have been anywhere in the setup, as long as it was placed before the photodiodes. Indeed, the influence of the optical and electro-optical components on a given wavelength does not depend on the width of the spectrum surrounding this wavelength, but only on the wavelength itself.
Since both photodiodes used for measurements are not only sensitive to 1500nm, the filter role is to eliminate stray light and thus eliminate an additional error source. The component is a bandpass filter and its behaviour is given in Fig.4.10.

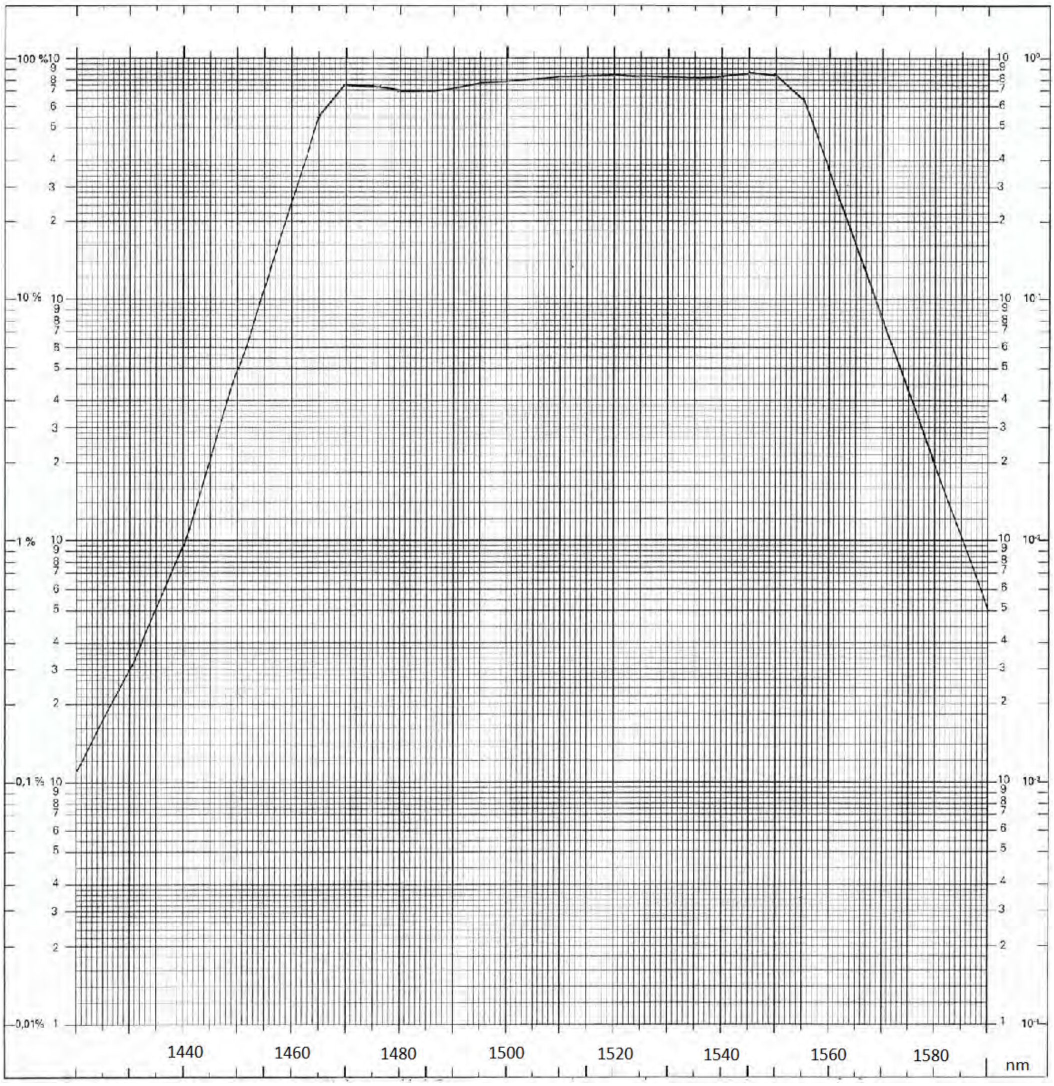

Figure 4.10: Filtering behaviour of the bk-1500-090-B bandpass filter (Interferenz Optik datasheet)

The spectrum after the filter lies between 1470nm and 1550nm with a transmission coefficient of approximately 70%. It reaches a peak for 1550nm with a 80% transmission coefficient.

After being filtered, the light beam passes through the LCVR (LCC1111-C, Thorlabs Inc). A picture is given in Fig.4.11 and its transmission as a function of the wavelength presented in Fig.4.12.

Figure 4.11: Picture of the LCC1111-C LCVR [25]

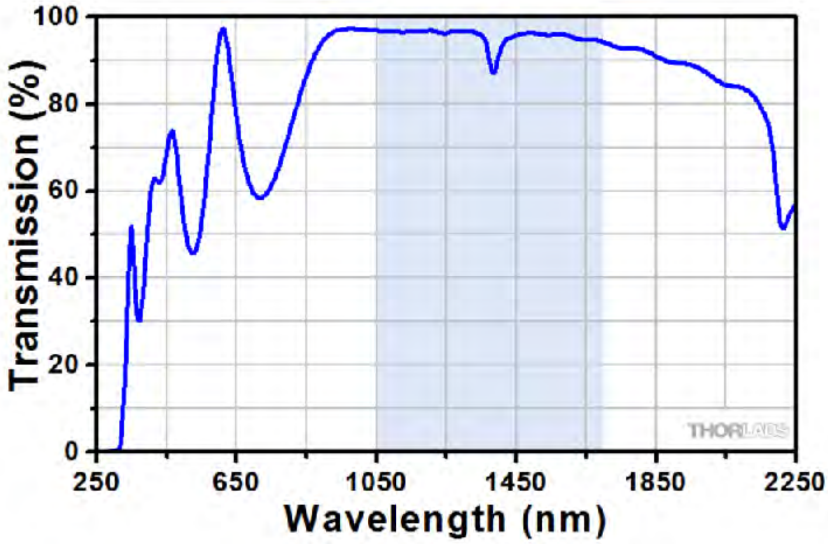

Figure 4.12: Transmission coefficient of the LCC1111-C LCVR as a function of the wavelength [26]

Since the aim is to work with approximately 1500nm, the LCVR is definetely appropriate, for its transmission coefficient is around 95% for this wavelength.
This component is an electro-optical device and is controlled by a square-wave voltage. Its behaviour depending on the voltage is shown in Fig.4.13.

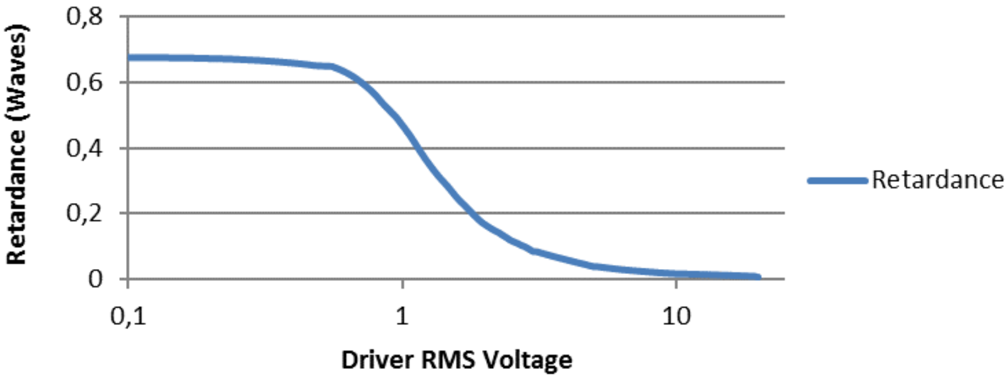

Figure 4.13: Phase shift induced between slow- and fast-axis of the LCC1111-C LCVR as a function of the RMS voltage for 25°C (Thorlabs datasheet)

One can see that the phase shift induced between its slow- and fast-axis can be monitored by varying the RMS voltage. More details on the LCVR monitoring are given in section 4.3.2.
Its advantage lies in it being electrically controlled. By varying the voltage, not only the phase shift but also the Mueller matrix of the PSA is changed. Section 4.2 introduces this matrix as a function of the LCVR voltage.

Once the linear polarised light is altered by the LCVR, it meets a non-polarising beam-splitter (CCM5-BS018/M, Thorlabs Inc) with a ratio of 50:50 (according to Thorlabs' technicians, the splitting-ratio slightly depends on the polarisation of the incident light beam and can vary by up to 10%). This component allows for the measurement of the full intensity at one output (photodiode 1) and further calculation on the outgoing light at the second output (analyser and then photodiode 2). A picture is given in Fig.4.14.

Figure 4.14: CCM5-BS018/M non-polarising beam-splitter [27]

For technical reasons, the analyser is actually a beam-splitter (same component as the polariser). Only one of its outputs is used, and as its name suggests, allows for the analysis of the incoming state of polarisation. Indeed, depending on the state of polarisation generated by the PSG and then altered by the LCVR, the analyser yields crucial informations on the linear part of the incoming light. As explained in section 3.2, the combination of informations collected before (photodiode 1) and beyond the analyser (photodiode 2) allows for the determination of the linear state of polarisation of the unknown infrared radiation.

The two last components of the assembly are the photodiodes (G12180-010A, Hamamatsu). They are presented in Fig.4.15.

Figure 4.15: Picture of a G12180-010A Hamamatsu photodiode [28]

The role of photodiode 1 is to measure the full intensity of the signal before it reaches the analyser. It would have been more appropriate to place it right after the PSG, but for technical reasons, it is located after the LCVR. Since the latter has a transmission coefficent around 95% (regardless of the incident state of polarisation), the full intensity of the incident light beam can be easily derived.
The photodiode 2 allows for the measurement of the intensity altered by the analyser. Its position has to be as close to the analyser as possible, so that the optical paths 1 and 2 almost have the same length. As a matter of fact, some loss due to the divergence of the light beam arises between the non-polarising beam-splitter and the photodiode 2. They are hard to derive, since losses already come from the rough splitting-behaviour of the non-polarising beam-splitter and also from the analyser transmission.
The sensitive area of both photodiodes has a diameter of 1mm. Since the light beam emerging from the lens approximately has the diameter of the lens (25.4mm), one can consider that the components alignement is precise enough, so that the whole sensitive surface of each photodiode is covered by the beam.

Additionally, one can see on Fig.4.2 that the non-polarising beam-splitter is covered with a black piece of paper. Indeed, the adaptor machined to hold the photodiode 1 is transparent and hence induces a leakage due to the surroundings infrared light. If this leakage were constant, it would not be a problem, as it would only be necessary to remove the offset from the signal of the photodiode. Nevertheless, the laboratory is an open space, and the weather influence on the daylight is significant. One has to keep in mind, that the assembly used in this Master's Thesis is an experimental set-up. Its final version should be fully covered.

To summarise:

- One has to split PSG and PSA in two independant parts, even if the PSA is located between two PSG components.
- The role of the PSG is to simulate a linear polarisation and the PSA analyses it.
- It is important to imagine two different optical paths in the PSA. The optical path 1 leads to photodiode 1 and the optical path 2 to photodiode 2. Those two optical paths do not have the same length and are not exactly composed of the same components.

4.2 Mathematical description of the optical setup

Another way to describe an optical assembly is to give its **Mueller matrix**. In this part, we are interested in determining the Mueller matrix of the sequence of optical and electro-optical devices along optical path 2. As a matter of fact, the signal received by the photodiode 1 does not require further matrix computation, since it almost directly (without matrix inversion) yields the full intensity of the incident light beam.

The full Mueller matrix of the setup is then the combination of a LCVR (see section 3.3) with an analyser (see section 3.1.3) and can be written as (4.1):

$$\mathbf{M} = \begin{pmatrix} 1 & 0 & 0 & 0 \\ 0 & C^2 + S^2\cos(\delta(V)) & SC(1-\cos(\delta(V))) & -S\sin(\delta(V)) \\ 0 & SC(1-\cos(\delta(V))) & C^2 + S^2\cos(\delta(V)) & C\sin(\delta(V)) \\ 0 & S\sin(\delta(V)) & -C\sin(\delta(V)) & \cos(\delta(V)) \end{pmatrix} \tag{4.1}$$

As explained in section 3.2, only the first line of the Mueller matrix (here **M**) is required for the polarisation state derivation. Let us first write matrix **A** (as defined in section 3.2) and explain why it is, in our case, not invertible. For three different voltages V_1, V_2 and V_3, we can get the three rows of **A** (4.2):

$$\mathbf{A} = k \begin{pmatrix} 1 & C^2 + S^2\cos(\delta(V_1)) & SC(1-\cos(\delta(V_1))) \\ 1 & C^2 + S^2\cos(\delta(V_2)) & SC(1-\cos(\delta(V_2))) \\ 1 & C^2 + S^2\cos(\delta(V_3)) & SC(1-\cos(\delta(V_3))) \end{pmatrix} \tag{4.2}$$

where k is the combination of the transmission coefficients of LCVR and analyser, $C = \cos(2\theta)$, $S = \sin(2\theta)$, θ is the angle between fast axis of the LCVR and an arbitrary plane (the horizon for example) and δ is the phase shift induced by the LCVR, which is a function of the voltage.

Actually, one can notice that the matrix **A** cannot be inverted. Using the trigonometrical relationship $C^2 + S^2 = 1$, we can rewrite (4.2) as follows:

$$\begin{aligned}
\mathbf{A} &= k \begin{pmatrix} 1 & 1 - S^2 + S^2\cos(\delta(V_1)) & SC(1-\cos(\delta(V_1))) \\ 1 & 1 - S^2 + S^2\cos(\delta(V_2)) & SC(1-\cos(\delta(V_2))) \\ 1 & 1 - S^2 + S^2\cos(\delta(V_3)) & SC(1-\cos(\delta(V_3))) \end{pmatrix} \\
&= k \begin{pmatrix} 1 & 1 - S^2(1-\cos(\delta(V_1))) & SC(1-\cos(\delta(V_1))) \\ 1 & 1 - S^2(1-\cos(\delta(V_2))) & SC(1-\cos(\delta(V_2))) \\ 1 & 1 - S^2(1-\cos(\delta(V_3))) & SC(1-\cos(\delta(V_3))) \end{pmatrix}
\end{aligned} \tag{4.3}$$

By substracting the first column to the second one, we get a column vector which is collinear to the third column. This is the reason why the matrix $\mathbf{A}$ is not invertible. This collinearity cannot be avoided by variating the voltages V_1, V_2 or V_3 or by changing the LCVR or analyser inclination. It is only a consequence of the setup optical behaviour. That is the reason why we will not work with the matrix $\mathbf{A}$ but with the 2×2 matrix $\mathbf{B}$. The latter is then given by:

$$\mathbf{B} = k \begin{pmatrix} C^2 + S^2\cos(\delta(V_1)) & SC(1-\cos(\delta(V_1))) \\ C^2 + S^2\cos(\delta(V_2)) & SC(1-\cos(\delta(V_2))) \end{pmatrix} \tag{4.4}$$

Let us verify that the matrix $\mathbf{B}$ is invertible by computing its determinant:

$$\begin{aligned}
\det(\mathbf{B}) &= k \begin{vmatrix} C^2 + S^2\cos(\delta(V_1)) & SC(1-\cos(\delta(V_1))) \\ C^2 + S^2\cos(\delta(V_2)) & SC(1-\cos(\delta(V_2))) \end{vmatrix} \\
&= k \begin{vmatrix} 1 - S^2(1-\cos(\delta(V_1))) & SC(1-\cos(\delta(V_1))) \\ 1 - S^2(1-\cos(\delta(V_2))) & SC(1-\cos(\delta(V_2))) \end{vmatrix}
\end{aligned} \tag{4.5}$$

For the sake of simplicity, let us now call $\cos(\delta(V_1)) = a$ and $\cos(\delta(V_2)) = b$. We can rewrite the determinant as:

$$\det(\mathbf{B}) = k \begin{vmatrix} 1 - S^2(1-a) & SC(1-a) \\ 1 - S^2(1-b) & SC(1-b) \end{vmatrix} \tag{4.6}$$

We then multiply the second column by $\frac{S^2}{SC}$ and add it to the first column:

$$\det(\mathbf{B}) = k \begin{vmatrix} 1 & SC(1-a) \\ 1 & SC(1-b) \end{vmatrix} \tag{4.7}$$

As long as $S \neq 0$, $C \neq 0$ and $a \neq b$ (which means $\cos(\delta(V_1)) \neq \cos(\delta(V_2))$), the matrix $\mathbf{B}$ is invertible. Since we are choosing two voltages so that $V_1 \neq V_2$, we just have to pay attention that the phase shift introduced by the LCVR for V_1 is not the opposite of the phase shift introduced for V_2. Mathematically speaking, we do not want: $\delta(V_1) = -\delta(V_2)$.
Matrix $\mathbf{B}$ is then invertible and its definition is given in (4.3). One can notice that $\mathbf{B}$ is a function of the voltage, since the phase shift induced by the LCVR depends on the voltage applied on its electrodes. That is the reason why only its formal version is given in (4.3).

So far, the LCVR azimuthal angle θ is not defined. This orientation plays a major role in the assembly efficiency. Indeed, its value has a direct influence on matrix $\mathbf{B}$ capacity to be inverted. Without mathematical computation and simply by logical reasoning, already two LCVR azimuthal angles (orientation of its fast-axis) can be excluded: 0°and 90°(their exclusion is already mathematically proven in the previous paragraph since $S = \sin(2\theta) \neq 0$). Let us imagine that the LCVR fast-axis angle is 0°. This means that the LCVR fast-axis and the analyser have the same orientation angle. Let us also take two linear states of polarisation which are symmetrical to the horizon (for example +30° and −30°). After their passage through the LCVR, regardless of the phase shift induced by the LCVR, the two polarisation states after the LCVR will still be symmetrical to the fast-axis. With this in mind, the analyser then sees two polarisation states, which are symmetrical to its own orientation angle, and thus cannot differentiate them.
The same problem occurs when the LCVR slow-axis (not fast-axis this time) coincides with the analyser orientation angle. As a matter of fact, let us set the fast-axis vertically (90° angle). Let us then imagine two linear states of polarisation generated by the PSG which are symmetrical to the vertical (70° and 110° for example). After their passage through the LCVR, they will still be symmetrical to the vertical, and thus the horizontal analyser will not see any difference beetwen the two of them.
Mathematically speaking, one can also exclude the angle of $\theta = 45°$. As a matter of fact, the latter would yield a value of $S = \cos(2\theta) = 0$. Hence, Matrix $\mathbf{B}$ determinant is equal to zero and $\mathbf{B}$ is singular.
The question is then: what is the best LCVR azimuthal angle? According to [11], θ should be equal to 27.37°. Nevertheless, the azimuthal angle will be taken here as equal to 22.5°. As a matter of fact, the LCVR holder already presents a central circle with four holes around it for the four shafts. Those holes are set to angles of 45°, 135°, −135° and −45° to the horizon. It is easier to equally split one eighth of a circle (between 0° and 45°) in two and thus set the LCVR to an angle of 22.5°.

4.3 Electronics of the system

4.3.1 Acquisition of the signals

The signals were acquired with a USB-6009 National Instruments data acquisition device (Fig.4.16).

Figure 4.16: Picture of the USB-6009 data acquisition device [29]

The latter presents 8-analog inputs (14-bit, 48kS/s), functioning in a voltage range between -10V and +10V. Since the signals coming from the photodiodes are quite low (few hundreds of mV), they are amplified to several volts. The amplifier (already developed for another diploma work [30]) is presented in Fig.4.17.

Figure 4.17: Picture of the amplifier

Two of its inputs are connected to the two photodiodes and the same level of amplification at its outputs is used for both signals.

The signals are computed thanks to the software LabVIEW, using a basic acquisition program presented in Fig.4.18.

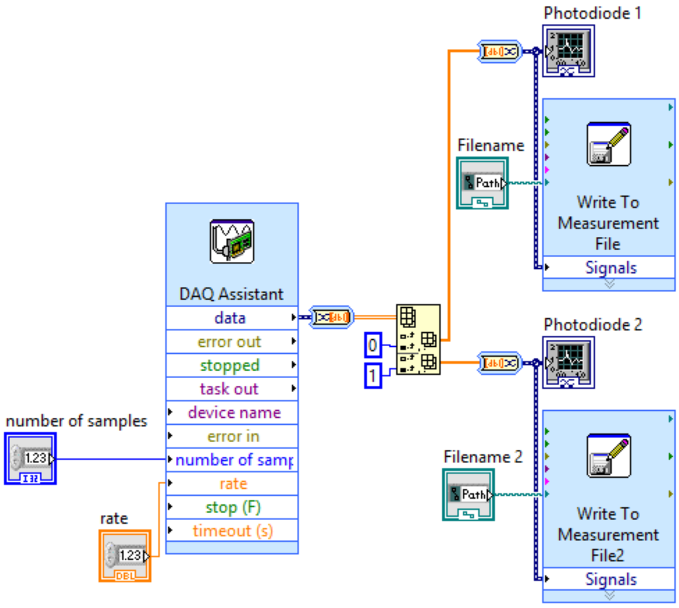

Figure 4.18: Block diagram of the LabVIEW acquisition program

Each measurement is performed at a 1kHz rate, during 10s. As a matter of fact, the radiation of the IR-emitter tends to oscillate with time, and shorter aquisition times could have been corrupted by this oscillation. The signal is not filtered, as the noise (certainly emerging from electromagnetic interference, since its frequency lies between 50Hz and 60Hz) is random and thus has a zero mean value. Fig.4.19 shows the example of an intensity measurement on photodiode 1.

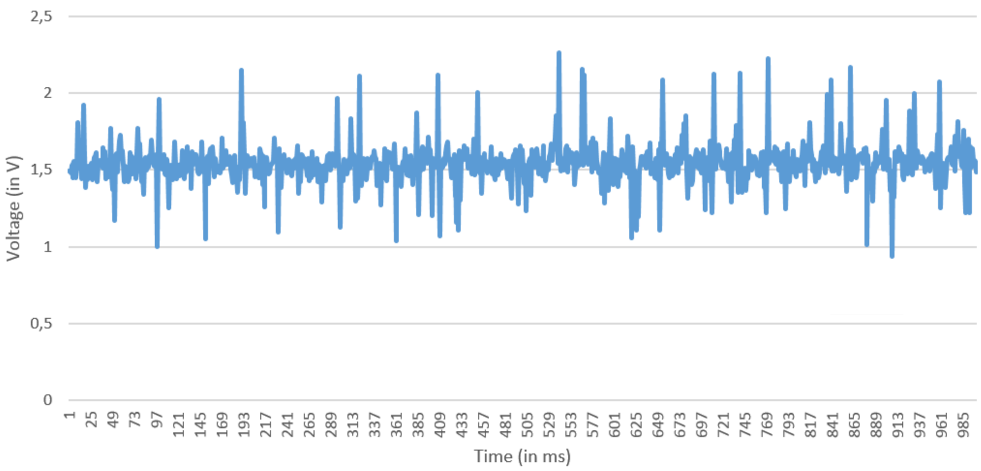

Figure 4.19: Electromagnetic noise on an intensity measurement acquired by photodiode 1 (1s, 1000 samples)

One can definitely see that the random noise actually has a frequency of approximately 50Hz.

4.3.2 Monitoring of the components

Several devices have to be monitored: the IR-emitter, the LCVR and the amplifier. Fig.4.20 introduces the intensity and voltage to be chosen for the IR-emitter.

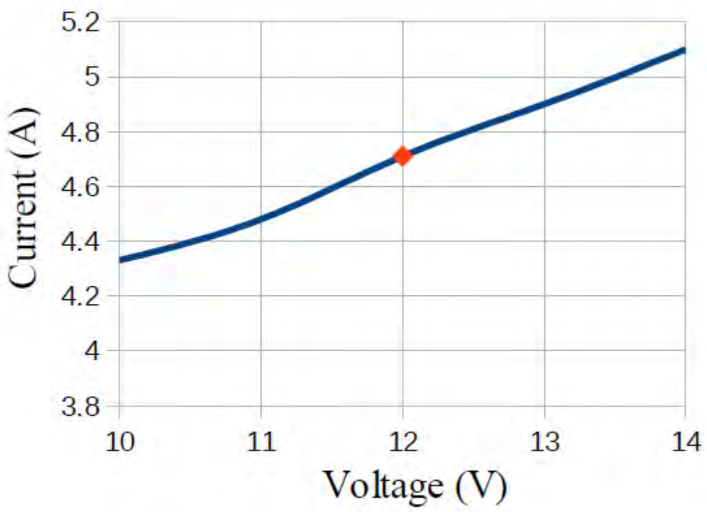

Figure 4.20: Monitoring characteristics of the IR-emitter (Hawkeye Technologies datasheet)

However, the behaviour presented in Fig.4.20 is an ideal case. Probably due to the generator limitation or the emitter aging, the power supplied to the device does not exceed an average of 41W, whereas the informations provided by the manufacturer clearly indicate an average power of 56W (this value can be obtained at any point of the curve since it is linear). This deviation makes it hard to evaluate the radiating body temperature, since all the informations are given for a power of 56W. Nevertheless, the IR-emitter still radiates enough intensity for the sake of the experiment.

As explained in section 3.3, the LCVR needs to by driven by an alternating voltage. The latter actually is a square signal of 2kHz. According to the manufacturer, the frequency has to be at least over 1kHz, with an optimal behaviour for 2kHz. The phase shift induced by the device only depends on the RMS (Root Mean Square) value of the voltage. For a square signal without offset, the RMS then simply corresponds to the voltage positive peak value.
The LCVR admits a voltage between 0V and 25V without offset. Each of the RMS value corresponds to a certain phase shift, offering a variable behaviour from a half-wave plate (180° phase shift) up to an almost transparent inactive device (0° phase shift). Actually,

without voltage and for a wavelength of 1550nm, the phase shift is approximately 241°, whereas the medium is almost inactive for 25V (2.52° phase shift). Further informations on the phase shift as a function of the RMS voltage value are given in Fig.4.13.

4.3.3 Data processing of the signals

All of the data where saved in LabVIEW as .TDMS files. This extension allows for a further extrapolation of the data in Excel. The latter was only used to compute series of numbers mean values. As a matter of fact, each acquired signal does not variate much over time and can be averaged. Attention has to be paid to the offset of each photodiode. That is the reason why, prior to each measurement, this offset is computed for each photodiode and substracted from the signals.

Once the mean values are computed, they can be reused for the polarisation state determination. This derivation is realised by a MATLAB program given in Fig.4.21.

```
clear all; close all; clc;

% This program computes the value of the linear polarised incident Stokes
% vector as well as the azimuth angle of the linear polarisation.
% It requires the full intensity (photodiode 1) and the intensity of
% photodiode 2 for two different voltages on the LCVR.

% Definition of some constants
theta=(22.5/360)*2*pi;  % Angle between fast-axis of LCVR and horizon
C=cos(2*theta);         % Constant for simplification of matrix B
S=sin(2*theta);         % Constant for simplification of matrix B

%Transmission coefficient of the Analyser
c=0.98;

% Choice of the phase-shift introduced by the LCVR (in radian) for the 2
% different voltages
delta_1=0.53*2*pi;  %RMS=1V
delta_2=0.16*2*pi;  %RMS=2V

% Creation of the Matrix B
B=0.5*[ C^(2)+S^(2)*cos(delta_1) S*C*(1-cos(delta_1));
        C^(2)+S^(2)*cos(delta_2) S*C*(1-cos(delta_2))];

% Definition of values required to build vector J
S_out_0_V1=1.31/c;  % Intensity measured by photodiode 2 for delta_1
S_out_0_V2=0.92/c;  % Intensity measured by photodiode 2 for delta_2
a11_V1=0.5;         % Coefficient (1,1) of matrix A(V1)
a11_V2=0.5;         % Coefficient (1,1) of matrix A(V2)
S_in_0=1.34;        % Full intensity measured by photodiode 1

% Build-up of vector J
J=[S_out_0_V1-a11_V1*S_in_0;
   S_out_0_V2-a11_V2*S_in_0];

% Computation of the incident state of polarisation
I=inv(B)*J;         % I contains the second and third values of the
                    % incident Stokes vector.
S_in_1=I(1);
S_in_2=I(2);
S=[S_in_0;
   S_in_1;
   S_in_2]/S_in_0   % Build-up and normalisation of the incident Stokes
                    % vector S

% Computation of the azimuth angle of the linear polarisation
alpha=atan(sqrt((S_in_0-S_in_1)/(S_in_0+S_in_1)))*360/(2*pi)
```

Figure 4.21: MATLAB program for the polarisation state determination

Some explanations must be given on it:

- **lines 9 to 11**: some constants are declared. *theta* is the azimuth angle of the LCVR fast-axis. C and S allows for the simplification of matrix **B**.
- **line 14**: c stands for the transmission coefficient of the analyser. Indeed, the optical path 2 runs through the analysing beam-splitter which has its own transmission. According to Thorlabs, the latter can be approximated around 98%.
- **lines 18 to 19**: *delta*_1 and *delta*_2 represent the phase shift (in radian) respectively for V_1 and V_2 induced by the LCVR. For each possible RMS value of the voltage, the phase shift can be found in the component datasheet. In Fig.4.21, a RMS of 1V and 2V respectively induces a phase shift (in waves) of 0.53 and 0.16.
- **lines 22 to 23**: matrix **B** is created using the shortened variables C and S.
- **lines 26 to 27**: the intensities $S\_out\_0\_V1$ and $S\_out\_0\_V2$ measured by photodiode 2 respectively for V_1 and V_2 need to be increased (because of the transmission of the analyser) and thus divided by c.
- **lines 28 to 29**: the first coefficient a_{11} of matrix **A** is defined for the voltage V_1 as $a11\_V1$ and for V_2 as $a11\_V2$.
- **line 30**: the intensity measured by photodiode 1 defines the full intensity of the source. It does not need any division by the transmission coefficient c since no analyser is involved in the optical path 1.
- **lines 33 to 34**: vector $\vec{J}$ (defined in (3.26)) is built up.
- **line 37**: according to (4.7), matrix **B** is invertible. Thus, $\vec{I}$ can be computed. The latter is a column vector containing the second Stokes parameter S_in_1 in its first row and the third one S_in_2 in its second row.
- **lines 39 to 43**: the unknown incident Stokes vector S is built up and normalised (division by its first component S_in_0).
- **line 47**: thanks to a mathematical relation between the azimuth angle of the linear polarisation and the components of the Stokes, this azimuth angle *alpha* can be derived.

The computation of the azimuth angle *alpha* of the incident linear polarisation is a good way to verify the functionning of the assembly. As a matter of fact, each linear polarisation state generated by the PSG has its own Stokes vector. The derivation of the latter is complicated (except in some particular cases presented in section 3.1.2) and does not give much physical understanding of the results.

4.4 Budget for the assembly

Including a budget in this Master's Thesis is important, for the project should be further investigated and hopefully, the results presented here will be reused. This budget only comprises the price of the different optical components, at the time they were bought. It does not include the power generator for the IR-emitter nor the voltage generator necessary for the LCVR monitoring nor the data acquisition device. The prices of the different wires, holders, adaptors (some of them were machined in the laboratory), screws, shafts of the optical assembly and the optical rail is also excluded. Indeed, they can vary from one setup to another. The following Tab.4.1 details the assembly price.

Ref	**Qty**	**Unit price** (in €)	**Total price** (in €)	**Source**
Si295 IR-Emitter	1	130.79	130.79	Scitec Instruments Ltd
LA4306, unmounted lens	1	87.57	87.57	Thorlabs, Inc
bk-1500-090-B, interference filter	1	259.00	259.00	Interferenzoptik Elektronik GmbH
LCC1111-C, LCVR	1	562.50	562.50	Thorlabs, Inc
CCM5-BS018/M, non-polarising beam-splitter	1	178.20	178.20	Thorlabs, Inc
CCM1-PBS254/M, polarising beam-splitter	2	269.10	538.20	Thorlabs, Inc
G12180-010A, photodiode	2	84.00	168.00	Hamamatsu
			1924.26	

Table 4.1: Budget of the optical assembly
(All prices are given without VAT. For some components, the price in € is given for a GBP/Euro exchange rate of 1£= 1.17€. Prices might vary with time.)

It is important to notice that the total amount only includes the price of the optical and electro-optical devices. One also has to add the different softwares used for computation (Excel, LabVIEW and MATLAB).

5 Experiments

5.1 Determination of the focal length of the lens

The PSA first component is the lens. It allows for the source light focus into a parallel beam. In order to place it properly in the assembly, one must derive its focal length. As a matter of fact, the latter is not given for 1500nm and changes for each wavelength. Additionally, optical distances are not always related to surfaces one could easily measure. All this complicates the computation of correct distances. The focal length somehow has to be derived.

The idea is to generate a **non-polarised** point source (here the IR-emitter) and to move the lens until both signals of photodiode 1 and photodiode 2 are equal. Indeed, when the right lens position is reached, the emitter tip is located in the object focal point and hence all rays of the point source are parallel to each other in the PSA. The intensity measured by both photodiodes is then independant of each optical path length. Since the source is unpolarised, the analyser does not alterate the intensity of the beam. For this particular lens position, photodiodes 1 and 2 yield the same intensity.

Before exactly finding the right lens position, the focal point is roughly indentified by visually comparing both photodiode signals on the oscilloscope. It seems to be located between 56mm and 75mm. In order to find it more precisely, a serie of measurements is carried out between 56mm and 75mm with a step of 1mm (optical rail scale). The results are presented in Tab.5.1.

d (in mm)	56	57	58	59	60	61	62	63	64	65
I_1**(in V)**	1.85	1.81	1.78	1.77	1.65	1.71	1.61	1.45	1.57	1.58
I_2**(in V)**	2.25	2.17	2.10	2.03	1.88	1.88	1.74	1.52	1.61	1.58
$c = \frac{I_1}{I_2}$	0.82	0.84	0.85	0.87	0.88	0.91	0.93	0.95	0.98	1.00
d	66	67	68	69	70	71	72	73	74	75
I_1**(in V)**	1.53	1.58	1.54	1.49	1.48	1.45	1.43	1.43	1.43	1.40
I_2**(in V)**	1.49	1.49	1.40	1.32	1.29	1.24	1.21	1.14	1.16	1.10
$c = \frac{I_1}{I_2}$	1.03	1.06	1.10	1.13	1.15	1.17	1.18	1.25	1.24	1.27

Table 5.1: Intensity of both photodiodes as a function of the lens position (**d** stands for the distance between tip of the IR-emitter and lens flat surface, I_1 and I_2 are the intensities measured respectively by photodiode 1 and photodiode 2 and c is the ratio between I_1 and I_2)

On Tab.5.1 one can see that the right lens position is 65mm. Indeed, for this position, **c** is exactly equal to one.

5.2 Determination of the state of polarisation

The aim of the Master's Thesis is to measure the polarisation state of linear polarised radiation. In order to check if the assembly works, some linear polarisation states are generated by the PSG and analysed by the PSA. One must know that the whole polarisation range is fully defined between $-90°$ and $90°$. As a matter of fact, linear polarisation states are symmetrical around the wave propagation axis (see Fig.3.2).
Since there are infinite various linear polarisation states between $-90°$ and $90°$, some particular polarisation angles are chosen from $-90°$ to $90°$ with a step of $22.5°$. There is no need to proceed to measurements for $-90°$ since the related polarisation state is the same for $90°$. The Stokes vectors for $0°$, $45°$ and $90°$ are well known and already introduced in Tab.3.2. The others can easily be computed using the equations given in section 3.1.2.

Each polarisation state measurement relies on the choice of a couple of voltages (V_1 and V_2) driving the LCVR. Because of the almost infinite various combinations of V_1 and V_2, three distinct pairs of values are chosen:

- pair 1: $V_1 = 0V$ and $V_2 = 2V$
- pair 2: $V_1 = 2V$ and $V_2 = 10V$
- pair 3: $V_1 = 0V$ and $V_2 = 10V$

$0V$ and $10V$ correspond to the two LCVR phase shift extrema ($0V$ and $10V$) reachable with the power generator. The third voltage ($2V$) yields a phase shift inbetween (see Fig.4.13), close to the phase shift curve inflection point.
The induced phase shifts for $0V$, $2V$ and $10V$ depend on the wavelength. Tab.5.2 sumarizes them for 1310nm and 1550nm (only accessible values on Thorlabs datasheet). The computed deviation is the absolute value of the difference between phase shifts for 1550nm and 1310nm.

	0V	**2V**	**10V**
Phase shift for 1310nm	270.36°	58.32°	11.16°
Phase shift for 1550nm	227.52°	57.60°	9.36°
Deviation	42.84°	0.72°	1.80°

Table 5.2: Influence of the wavelength on LCVR phase shifts for 0V, 2V and 10V

Since the spectrum in the PSA reaches a peak for 1550nm (Fig.4.10), one can make the approximation that the LCVR phase shift values can be taken for 1550nm. The results presented in the following three tables (Tab.5.3, Tab.5.4 and Tab.5.5) are then derived with LCVR phase shifts for 1550nm at $25°C$. Some definitions must be given for the understanding of each table:

- actual polarisation angle: ϕ_a
- computed polarisation angle: ϕ_c

- angular deviation: $\delta_{phi} = |\phi_a - \phi_c|$
- actual Stokes vector: $\vec{S_a} = \begin{pmatrix} S_{a;0} \\ S_{a;1} \\ S_{a;2} \end{pmatrix}$
- computed Stokes vector: $\vec{S_c} = \begin{pmatrix} S_{c;0} \\ S_{c;1} \\ S_{c;2} \end{pmatrix}$
- root-mean-square deviation [31]: $\delta_{RMSD} = \sqrt{\frac{(S_{a;0}-S_{c;0})^2+(S_{a;1}-S_{c;1})^2+(S_{a;2}-S_{c;2})^2}{3}}$.

Tab.5.3 presents the derivation of the above mentionned generated incident linear states of polarisation for voltage pair 1 (0V;2V).

Actual polarisation angle ϕ_a	**Computed polarisation angle** ϕ_c	**Angular deviation** δ_{phi}	**Actual Stokes vector** $\vec{S_a}$	**Computed Stokes vector** $\vec{S_c}$	**Root-mean-square deviation** δ_{RMSD}
$-67.5°$	$-57.41°$	$10.09°$	$\begin{pmatrix} 1 \\ -\frac{1}{\sqrt{2}} \\ -\frac{1}{\sqrt{2}} \end{pmatrix}$	$\begin{pmatrix} 1 \\ -0.42 \\ -0.68 \end{pmatrix}$	0.09
$-45°$	$-37.17°$	$7.83°$	$\begin{pmatrix} 1 \\ 0 \\ -1 \end{pmatrix}$	$\begin{pmatrix} 1 \\ 0.27 \\ -0.81 \end{pmatrix}$	0.11
$-22.5°$	$-16.43°$	$6.07°$	$\begin{pmatrix} 1 \\ \frac{1}{\sqrt{2}} \\ -\frac{1}{\sqrt{2}} \end{pmatrix}$	$\begin{pmatrix} 1 \\ 0.84 \\ -0.60 \end{pmatrix}$	0.06
$0°$	$3.79°$	$3.79°$	$\begin{pmatrix} 1 \\ 1 \\ 0 \end{pmatrix}$	$\begin{pmatrix} 1 \\ 1.01 \\ -0.02 \end{pmatrix}$	0.01
$22.5°$	$15.01°$	$7.49°$	$\begin{pmatrix} 1 \\ \frac{1}{\sqrt{2}} \\ \frac{1}{\sqrt{2}} \end{pmatrix}$	$\begin{pmatrix} 1 \\ 0.87 \\ 0.54 \end{pmatrix}$	0.08
$45°$	$36.38°$	$8.62°$	$\begin{pmatrix} 1 \\ 0 \\ 1 \end{pmatrix}$	$\begin{pmatrix} 1 \\ 0.30 \\ 0.80 \end{pmatrix}$	0.12
$67.5°$	$58.32°$	$9.18°$	$\begin{pmatrix} 1 \\ -\frac{1}{\sqrt{2}} \\ \frac{1}{\sqrt{2}} \end{pmatrix}$	$\begin{pmatrix} 1 \\ -0.45 \\ 0.64 \end{pmatrix}$	0.09
$90°$	$83.47°$	$6.53°$	$\begin{pmatrix} 1 \\ -1 \\ 0 \end{pmatrix}$	$\begin{pmatrix} 1 \\ -0.97 \\ 0.05 \end{pmatrix}$	0.02

Table 5.3: Derivation of various incident linear polarisation states for voltage pair 1 (0V;2V), with LCVR phase shifts taken for 1550nm at 25°C

One can notice that the results give an approximation by several degrees of the actual polarisation angle. The latter always deviates by a few degrees, mostly for $-67.5°$ where the angular deviation is $10.09°$. Nevertheless, the optical assembly yields a good approximation for $0°$ ($3.79°$ angular deviation). The root-mean-square deviation is acceptable but quite high for $45°$ ($\delta_{RMSD} = 0.12$). Indeed, $S_{c;1} = 0.30$ for $45°$ whereas it should be close to zero.

Tab.5.4 shows the same computation as Tab.5.3 but for voltage pair 2 (2V;10V).

Actual polarisation angle ϕ_a	**Computed polarisation angle** ϕ_c	**Angular deviation** δ_{phi}	**Actual Stokes vector** $\vec{S_a}$	**Computed Stokes vector** $\vec{S_c}$	**Root-mean-square deviation** δ_{RMSD}
$-67.5°$	$-63.43°$	$4.07°$	$\begin{pmatrix}1\\-\frac{1}{\sqrt{2}}\\-\frac{1}{\sqrt{2}}\end{pmatrix}$	$\begin{pmatrix}1\\-0.60\\-0.71\end{pmatrix}$	0.04
$-45°$	$-40.40°$	$4.60°$	$\begin{pmatrix}1\\0\\-1\end{pmatrix}$	$\begin{pmatrix}1\\0.16\\-1.10\end{pmatrix}$	0.06
$-22.5°$	$-28.66°$	$6.16°$	$\begin{pmatrix}1\\\frac{1}{\sqrt{2}}\\-\frac{1}{\sqrt{2}}\end{pmatrix}$	$\begin{pmatrix}1\\0.54\\-0.51\end{pmatrix}$	0.09
$0°$	$8.35°$	$8.35°$	$\begin{pmatrix}1\\1\\0\end{pmatrix}$	$\begin{pmatrix}1\\1.04\\-0.13\end{pmatrix}$	0.05
$22.5°$	$19.60°$	$2.90°$	$\begin{pmatrix}1\\\frac{1}{\sqrt{2}}\\\frac{1}{\sqrt{2}}\end{pmatrix}$	$\begin{pmatrix}1\\0.77\\0.84\end{pmatrix}$	0.05
$45°$	$43.25°$	$1.75°$	$\begin{pmatrix}1\\0\\1\end{pmatrix}$	$\begin{pmatrix}1\\0.06\\1.58\end{pmatrix}$	0.19
$67.5°$	$64.89°$	$2.61°$	$\begin{pmatrix}1\\-\frac{1}{\sqrt{2}}\\\frac{1}{\sqrt{2}}\end{pmatrix}$	$\begin{pmatrix}1\\-0.64\\1.27\end{pmatrix}$	0.19
$90°$	$86.43°$	$3.57°$	$\begin{pmatrix}1\\-1\\0\end{pmatrix}$	$\begin{pmatrix}1\\-1.01\\0.16\end{pmatrix}$	0.05

Table 5.4: Derivation of various incident linear polarisation states for voltage pair 2 (2V;10V), with LCVR phase shifts taken for 1550nm at 25°C

The results obtained for voltage pair 2 (2V;10V) are more accurate than for voltage pair 1 (0V;2V). Except for the 0° linear polarisation state, all angular deviations are under 6.16°, whereas voltage pair 1 yielded approximations in the range of an average 8°. One can also notice that some Stokes vector components are way overestimated and lose their physical meaning, for example for 45° where $S_{c_2} = 1.58$, while it should be lower than one. The root-mean-square deviations for 45° and for 67.5° are both very high and equal to 0.19. The accuracy provided by voltage pair 2 is quite poor.

Tab.5.5 introduces the third set of results obtained for voltage pair 3 (0V;10V).

Actual polarisation angle ϕ_a	**Computed polarisation angle** ϕ_c	**Angular deviation** δ_{phi}	**Actual Stokes vector** $\vec{S_a}$	**Computed Stokes vector** $\vec{S_c}$	**Root-mean-square deviation** δ_{RMSD}
$-67.5°$	$-64.53°$	$2.97°$	$\begin{pmatrix} 1 \\ -\frac{1}{\sqrt{2}} \\ -\frac{1}{\sqrt{2}} \end{pmatrix}$	$\begin{pmatrix} 1 \\ -0.63 \\ -0.65 \end{pmatrix}$	0.03
$-45°$	$-41.55°$	$3.45°$	$\begin{pmatrix} 1 \\ 0 \\ -1 \end{pmatrix}$	$\begin{pmatrix} 1 \\ 0.12 \\ -0.91 \end{pmatrix}$	0.05
$-22.5°$	$-23.18°$	$0.78°$	$\begin{pmatrix} 1 \\ \frac{1}{\sqrt{2}} \\ -\frac{1}{\sqrt{2}} \end{pmatrix}$	$\begin{pmatrix} 1 \\ 0.69 \\ -0.79 \end{pmatrix}$	0.03
$0°$	$8.28°$	$8.28°$	$\begin{pmatrix} 1 \\ 1 \\ 0 \end{pmatrix}$	$\begin{pmatrix} 1 \\ 1.04 \\ -0.02 \end{pmatrix}$	0.01
$22.5°$	$19.51°$	$2.99°$	$\begin{pmatrix} 1 \\ \frac{1}{\sqrt{2}} \\ \frac{1}{\sqrt{2}} \end{pmatrix}$	$\begin{pmatrix} 1 \\ 0.77 \\ 0.55 \end{pmatrix}$	0.06
$45°$	$43.11°$	$1.89°$	$\begin{pmatrix} 1 \\ 0 \\ 1 \end{pmatrix}$	$\begin{pmatrix} 1 \\ 0.07 \\ 0.85 \end{pmatrix}$	0.06
$67.5°$	$64.80°$	$2.70°$	$\begin{pmatrix} 1 \\ -\frac{1}{\sqrt{2}} \\ \frac{1}{\sqrt{2}} \end{pmatrix}$	$\begin{pmatrix} 1 \\ -0.64 \\ 0.68 \end{pmatrix}$	0.02
$90°$	$86.60°$	$3.40°$	$\begin{pmatrix} 1 \\ -1 \\ 0 \end{pmatrix}$	$\begin{pmatrix} 1 \\ -1.01 \\ 0.059 \end{pmatrix}$	0.02

Table 5.5: Derivation of various incident linear polarisation states for voltage pair 3 (0V;10V), with LCVR phase shifts taken for 1550nm at 25°C

Voltage pair 3 yields way better results than voltage pair 1 and 2. Except for 0°, all angular deviations are under 3.45°. The root-mean-square deviations are more than acceptable since they are all inferior to 0.06.

Tab.5.6 summarises all results in order to directly compare voltage pair 1, 2 and 3 accuracies.

Actual polarisation angle ϕ_a	Voltage pair 1 (0V;2V) Angular deviation δ_{phi}	Voltage pair 1 (0V;2V) RMS deviation δ_{RMSD}	Voltage pair 2 (2V;10V) Angular deviation δ_{phi}	Voltage pair 2 (2V;10V) RMS deviation δ_{RMSD}	Voltage pair 3 (0V;10V) Angular deviation δ_{phi}	Voltage pair 3 (0V;10V) RMS deviation δ_{RMSD}
$-67.5°$	10.09°	0.09	4.07°	0.04	2.97°	0.03
$-45°$	7.83°	0.11	4.60°	0.06	3.45°	0.05
$-22.5°$	6.07°	0.06	6.16°	0.09	0.78°	0.03
0°	3.79°	0.01	8.35°	0.05	8.28°	0.01
22.5°	7.49°	0.08	2.90°	0.05	2.99°	0.06
45°	8.62°	0.12	1.75°	0.19	1.89°	0.06
67.5°	9.18°	0.09	2.61°	0.19	2.70°	0.02
90°	6.53°	0.02	3.57°	0.05	3.40°	0.02

Table 5.6: Comparison of voltage pairs 1, 2 and 3 accuracy with LCVR phase shifts taken for 1550nm at 25°C

One can definetely see that voltage pair 3 yields more accurate results than pairs 1 and 2. Nevertheless, a quite high angular deviation remains for 0° when evaluated with voltage pair 3. Because of their high angular and root-mean-square deviations, one should not work with voltage pairs 1 and 2.
One must keep in mind that all results are approximations of actual Stokes vectors and polarisation state angles. One interrogation remains: where do all deviations come from? Next section 5.3 answers to this question.

5.3 Origins of the assembly inaccuracy

In section 5.2 the assembly seems to work, since the generated linear polarisation states are approximated in a range of several degrees. Nevertheless, all computed values deviate from the actual ones. The aim of this section 5.3 is to find where those inaccuracies come from.

The first deviation source is the lens positioning. As a matter of fact, one can already see the influence of a 1mm displacement on the source rays focus (Tab.5.1). As a matter of fact, the right lens position is assumed to be approximately 65mm and corresponds to the point where both photodiodes get the same intensity. By moving the lens of only 1mm, the ratio between both signals already changes from 1 to 1.03. This deviation surely has an influence on the assembly accuracy.

Another imprecision source is the LCVR azimuthal angle positioning. The fast axis is set to an angle of approximately 22.5° with the analyser (horizon). Nevertheless, the positioning precision can hardly reach more than a couple of degrees. In order to quantify its influence, let us take the intensity measurements for voltage pair 3 (0V;10V) and virtually variate the LCVR azimuthal angle value in the MATLAB program. Tab.5.7 presents this deviation in the computation of a 45° linear polarisation state.

o **Value to be derived**	**Derived value for an assumed LCVR fast-axis orientation of**				
	21.5°	22°	22.5°	23°	23.5°
Stokes vector	$\begin{pmatrix}1\\0.07\\0.85\end{pmatrix}$	$\begin{pmatrix}1\\0.07\\0.85\end{pmatrix}$	$\begin{pmatrix}1\\0.07\\0.85\end{pmatrix}$	$\begin{pmatrix}1\\0.07\\0.86\end{pmatrix}$	$\begin{pmatrix}1\\0.07\\0.86\end{pmatrix}$
RMSD	0.06	0.06	0.06	0.05	0.05
Polarisation angle	43.03°	43.03°	43.03°	43.03°	43.03°
Angular deviation	1.97°	1.97°	1.97°	1.97°	1.97°

Table 5.7: Influence of the LCVR azimuthal angle positioning accuracy on the derivation of a 45° linear Stokes vector for voltage pair 3 (0V;10V), with LCVR phase shifts taken for 1550nm at 25°C

According to Tab.5.7, the fast-axis positioning accuracy does not seem to have a strong influence on the results. One can notice that the derived Stokes vectors are the same for 21.5°, 22° and 22.5° and thus yield the same root-mean-square and angular deviation. In the case of 23° and 23.5°, only the third component S_2 undergoes an approximate 0.01 deviation. One has to find another source of inaccuracy.

After being filtered the analysed spectrum has a width of approximately 80nm (see Fig.4.10). Since the manufacturer only provides phase shifts for 1310nm and 1550nm, they have to be somehow computed in advance to suit the filter behaviour. In order to quantify the influence of a phase shift imprecision, let us modify the LCVR phase shift in the MATLAB program and see how results deviate. Tab.5.8 shows the derivation of a 45° linear polarisation state using voltage pair 3 (0V;10V) with five different 0V phase shift values: 0.62, 0.63, 0.64, 0.65 and 0.66 (in waves). For the sake of simplicity, the phase shift induced by 10V is assumed to be constant. Remember that the 0V phase shift used in section 5.2 is approximately 0.64 (in waves).

Value to be derived	Derived value for an assumed LCVR phase shift of				
	0.62	0.63	0.64	0.65	0.66
Stokes vector	$\begin{pmatrix}1\\0.07\\0.82\end{pmatrix}$	$\begin{pmatrix}1\\0.07\\0.84\end{pmatrix}$	$\begin{pmatrix}1\\0.07\\0.86\end{pmatrix}$	$\begin{pmatrix}1\\0.07\\0.89\end{pmatrix}$	$\begin{pmatrix}1\\0.07\\0.92\end{pmatrix}$
RMSD	0.06	0.06	0.06	0.05	0.05
Polarisation angle	43.02°	43.02°	43.03°	43.03°	43.04°
Angular deviation	1.98°	1.98°	1.97°	1.97°	1.97°

Table 5.8: Influence of the 0V induced phase shift accuracy on the derivation of a 45° linear Stokes vector for voltage pair 3 (0V;10V)

The influence of the phase shift accuracy is already more noticeable than for the LCVR fast-axis orientation. Nevertheless, the induced deviation remains quite small in comparison to the results inaccuracy in section 5.2.

All optical and electro-optical devices are set parallel to another. Nevertheless, the whole assembly is fixed using an optical rail and only two shafts instead of four. As a matter of fact, the size of the non-polarising beam-splitter prevents the crossing of more than two shafts. A tilt angle between components can already have an influence on the results.

According to Thorlabs, the CCM5-BS018/M non-polarising beam-splitter does not have an ideal behaviour, especially if the source is polarised. In that case, a deviation up to 10% between both outputs can appear. Thus the splitting ratio is not 50:50 anymore. A good way to quantify this polarisation dependancy is to proceed to intensity measurements on photodiode 1 (full intensity) for all linear Stokes vectors generated by the PSG and see if the intensity variates with the incident polarisation angle. Tab.5.9 presents this influence.

Incident polarisation angle	−67.5°	−45°	−22.5°	0°	22.5°	45°	67.5°	90°
Full intensity (in V)	1.37	1.39	1.38	1.36	1.33	1.29	1.31	1.34

Table 5.9: Influence of the incident polarisation angle on the non-polarising beam splitter behaviour

Indeed, one can already notice in Tab.5.9 that the non-polarising beam-splitter has a non-negligible influence on the outgoing full intensity, the two extrem values being here $1.29V$ and $1.39V$.
Let us then quantify the effect of this full intensity modification on the Stokes vectors determination. Tab.5.10 presents the derivation of a 45° linear Stokes vectors using $1.29V$ (minimum value), $1.33V$ (value used in section 5.2) and $1.39V$ (maximum value) full intensity values in MATLAB.

Full intensity (in V)	1.29	1.33	1.39
Derived 45° **Stokes vector**	$\begin{pmatrix} 1 \\ 0.10 \\ 0.97 \end{pmatrix}$	$\begin{pmatrix} 1 \\ 0.07 \\ 0.85 \end{pmatrix}$	$\begin{pmatrix} 1 \\ 0.02 \\ 0.83 \end{pmatrix}$
RMSD	0.03	0.06	0.06
Polarisation angle	42.08°	43.11°	44.36°
Angular deviation	2.92°	1.89°	0.64°

Table 5.10: Influence of the non-polarising beam-splitter imperfect behaviour on the MATLAB derivation of a 45° linear Stokes vector for voltage pair 3 (0V;10V)

It is noticeable from Tab.5.10 that the non-polarising beam splitter induces inaccuracies of several degrees as well as imprecisions in the root-mean-square deviation.

One last significant source of inaccuracies is the precision of polarisation state generation. As a matter of fast, the PSG polariser position is set by reference to a graduated circle. The latter is shown in Fig.5.1.

Figure 5.1: Graduated circle used to set the PSG polariser position for each generated polarisation state

This circle is glued on the PSG polariser holder. Its positionning has a precision of a few degrees, since it is manually set. Once the circle is fixed, the PSG polariser is manually rotated in order to generate each polarisation state. This step also has a precision within a few degrees. Together, all imprecisions sources seem to explain the results inaccuracy.

6 Continuation of the project

6.1 Enhancements to the setup

The assembly used in this Master's Thesis (PSG and PSA) yields good results but should be further studied and enhanced. The aim of this section is to present all parts of the setup which need to be studied in more detail.

The first kind of improvements involves the component positioning. First, a deeper study has to be carried out on the lens in order to find its focal length more accurately. Secondly, all components have to be precisely aligned, using four shafts instead of two. This will prevent the influence of tilt angles.

The second kind of enhancements is related to the monitoring and acquirement of signals. In a first instance, research has to be carried out on the LCVR phase shift values. As explained in section 5.3, those phase shifts depend on the wavelength. The improvement consists in computing them so that they suit the filtered wavelength. In a second phase, the whole computation must be fully automated. The idea is to create a single LabVIEW program simultaneously driving the LCVR and acquiring both photodiodes signals. It should also compute the mean values of each signal and perform the computations previously performed by MATLAB. Nevertheless, one condition remains in order to fully automate the assembly. The offset on both photodiodes either has to be set to zero or earlier computed and saved in the program in order to substract it from all polarisation state measurements.

A third stage of improvements consists in replacing the CCM5-BS018/M non-polarising beam splitter by a more accurate component. Indeed, its splitting ratio of 50:50 can deviate up to 60:40. According to Thorlabs technicians, one can use a Polka Dot Beamsplitter to correct this.

Mathematically speaking, it would be interesting to further investigate on the combination of analyser azimuthal angle with LCVR phase shifts. As a matter of fact, those parameters appear in matrix $\mathbf{B}$. The idea is to find the best combination in order to minimize the influence of imprecisions which are then multiplied by $\mathbf{B}^{-1}$. A hint for this is presented in [11].

Finally, the size of the assembly can be reduced by using shorter adapters and thus setting all components closer to another. On one side, the PSA will have higher intensities to measure. On the other hand, the system will be more compact and thus easier to mount on a robot arm.

6.2 Further aim of the project

All experiments conducted so far were carried out using a PSG, the latter producing fully linear polarised polarisation state. Nevertheless, the aim of the project is to be able to measure partially linear polarised Stokes vectors. There is nothing to change on the setup or in the MATLAB program. Theoretically, the PSA is able to work with partially linear polarised infrared radiation.

In a further step, the system has to be tested on a heated infrared radiating surface. As explained in section 3.4.2, one has to compute the ratio between p- and s-polarisation. Fig.6.1 shows the relation between p- over s-polarisation ratio and polarisation state.

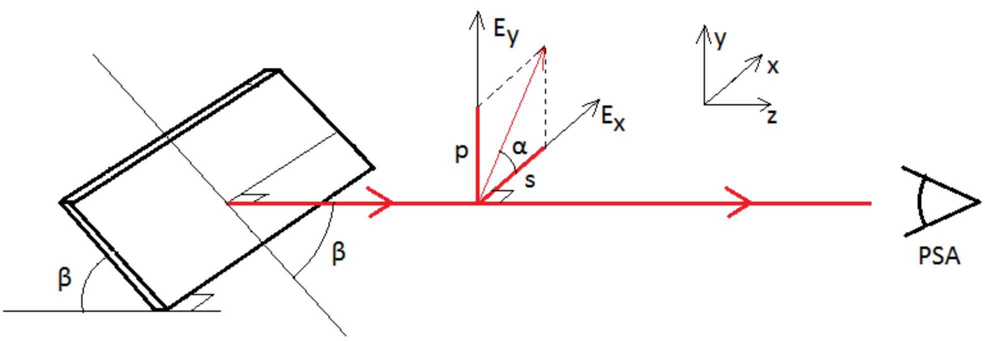

Figure 6.1: Scheme describing the relation between p- over s-polarisation ratio and polarisation state

The angle α and the length of the linear polarisation state yield enough informations to compute the p- over s-polarisation ratio. The computation is presented in (6.1):

$$\begin{aligned}
\frac{\epsilon(s-polarised)}{\epsilon(p-polarised)} &= \frac{1}{\tan(\alpha)} \\
&= \frac{1}{\tan(\arctan(\sqrt{|\frac{S_{in_0}-S_{in_1}}{S_{in_0}+S_{in_1}}|}))} \\
&= \frac{1}{\sqrt{|\frac{S_{in_0}-S_{in_1}}{S_{in_0}+S_{in_1}}|}} \\
&= \sqrt{|\frac{S_{in_0}+S_{in_1}}{S_{in_0}-S_{in_1}}|}
\end{aligned} \tag{6.1}$$

Once the ratio $\frac{\epsilon(s-polarised)}{\epsilon(p-polarised)}$ is known, one can simply extrapolate the value of β thanks to the curve (b) or (c) given in Fig.3.7. However, Fig.6.1 is an ideal case where p- and s-polarisation can clearly be identified. One must be sure that all right angles defined in Fig.6.1 are satisfied. Otherwise, the measured Stokes vector could yield biased informations due to other orientation angles around y- or z-axis of the radiating surface. One must also keep in mind that the radiating surface in Fig.6.1 is a plane and can be easily oriented to fit our coordinate system. The process is way more difficult to calibrate in reality.

Finally, the final step consists in mounting the PSA on a robot arm. This last stage requires more time than the one granted for the Master's Thesis. As a matter of fact, the assembly needs to be fitted to a system of multiple lenses already existing in the robot arm. As one can imagine, the positionning of all lenses could be tricky. The final mounted system is presented in Fig.6.2.

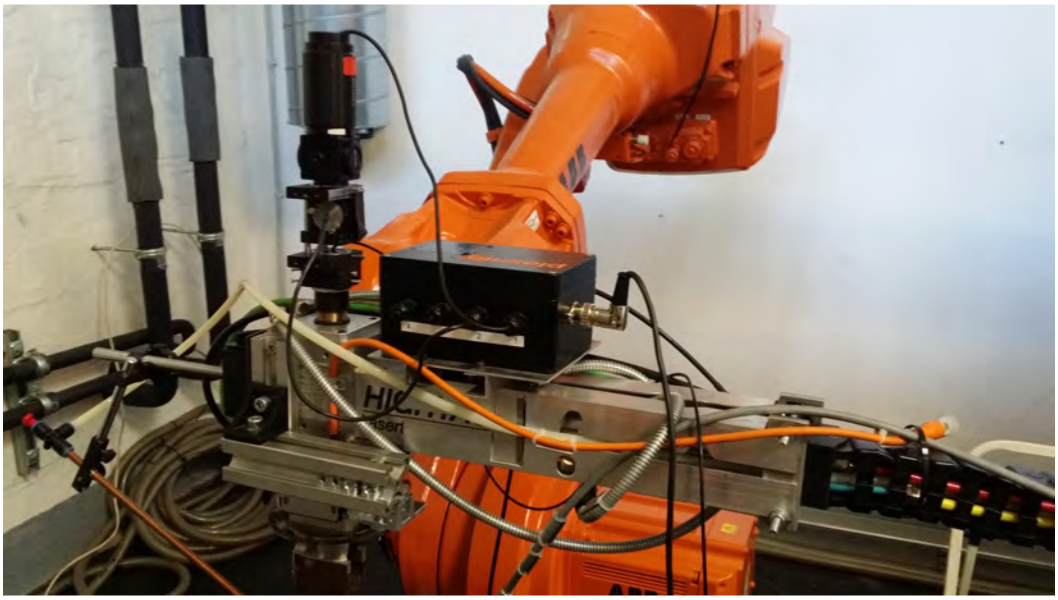

Figure 6.2: Assembly mounted on a laser cutting robot arm

This mounting allows for an in situ measurement of the polarisation state and thus tilt angle of a heated infrared radiating surface. Nevertheless, one has to keep in mind that a process generates smoke, which can on one hand cause deviations in measurements and thus in result accuracy and on the other hand reduce the infrared radiation intensity. Theoretically, the PSA created in this project is suitable for such experiments and should be further developped in order to finally fulfill its final purpose.

6.3 Alternative setups

Throughout the elaboration of the assembly, several problems were faced and solved. Nevertheless, in some cases, there were different solutions to these issues, which could have led to alternative setups.

As mentionned in section 4.1, the two optical paths respectively leading to photodiode 1 and 2 do not have the same length. This issue induces a loss of intensity due to the beam divergence, which is hard to quantify. An easy solution can be found by setting both photodiodes, so that optical paths 1 and 2 have the same length. In this particular case, the full intensity measured by photodiode 1 has undergone the same loss due to a beam divergence as the intensity measured by photodiode 2. Hence the intensity decrease between signal 1 and 2 only comes from the analyser influence and yields enough informations to compute the partially linear polarised incident Stokes vector. Furthermore, one could even get rid of the focusing lens. As a matter of fact, the lens was earlier used to solve the issue of beam divergence loss in case of optical paths with different lengths. Nevertheless the measured intensities are going to be way lower than with a lens. However, it would be interesting to undertake further study.

Photodiode 1 is used to yield informations on the full intensity since the beam does not meet any analyser along optical path 1. In case of fully linear polarised light, a system with only photodiode 2 is conceivable. One has to proceed to two measurements, respectively for two different LCVR voltages. It then remains to solve (3.28), where the degree of polarisation p is equal to 1. This solution is also applicable for partially linear polarised light whose polarisation degree p is already known.

One could also imagine an assembly with two LCVRs instead of one. Nevertheless, this second LCVR cannot replace the analyser. As a matter of fact, the variable retarders donnot have any influence on the measured intensity: they only change the polarisation state. The idea would then be to place the second LCVR right after the first one. The only difference I see is in the LCVRs monitoring. While previously two voltages (V_1 and V_2) had to be chosen, one can now separately drive the first LCVR only with V_1 and the second one with V_2. Nevertheless, I do not see the advantage of using two retarders since a single LCVR already yields enough informations on the incident lienar polarisation state. In case of a random state of polarisation (not only partially linear polarised), one LCVR is also sufficient. One simply has to drive it with an additional voltage V_3 and proceed to a mathematical derivation similar to the one carried out in section 5.2. However, the matrix $\mathbf{B}$ will be a 3×3 matrix.

7 Conclusion

As the title suggests, the aim of this Master's Thesis is to compute the polarisation state of partially linear polarised infrared radiation. All experiments in section 5 are led with fully linear polarised infrared radiation. Nevertheless, the assembly also works for partially linear polarised radiation, since it yields the full linear Stokes vector.

The time granted for this project was not sufficient to further investigate on measurements in situ, where the assembly is mounted on a robot arm. However, Fig.6.2 already gives a good impression of the final result.
There is still work to do on the setup full automation as well on the elaboration of a more compact system. Further studies should be more accurate in components positioning and polarisation state generation. It would also be interesting to mathematically find which is the best phase shift and analyser azimuthal angle combination.
Nevertheless, the results found with voltage pair 3 are more than acceptable. They only deviate by a few degrees and already give good approximations of incident Stokes vectors.

One has to keep in mind that all measurements were carried out with a punctual infrared radiating source. The latter causes troubles, which do not arise with visible laser light. As a matter of fact, one has to fight against beam divergence in an invisible wavelength range.

The assembly engineered in this Master's Thesis gives a new approach of process monitoring, for it can be employed in situ. Once deeper studied and optimised, it will allow for a better understanding and quality assessment of laser machining.

List of Figures

List of Tables

References

[1] MS Che Jamil et al. "Laser bending of pre-stressed thin-walled nickel micro-tubes". In: *Optics & Laser Technology* 73 (2015), pp. 105–117.

[2] Miroslav Radovanovic and Milos Madic. "Experimental investigations of CO2 laser cut quality: a review". In: *Nonconventional Technologies Review* 4 (2011), pp. 35–42.

[3] BS Yilbas. "Parametric study to improve laser hole drilling process". In: *Journal of Materials Processing Technology* 70.1 (1997), pp. 264–273.

[4] A Kaplan. "A model of deep penetration laser welding based on calculation of the keyhole profile". In: *Journal of Physics D: Applied Physics* 27.9 (1994), p. 1805.

[5] William M Steen. "Laser surface treatment". In: *Laser Processing: Surface Treatment and Film Deposition*. Springer, 1996, pp. 1–19.

[6] S. Hashmi. *Comprehensive Materials Processing*. Elsevier Science & Technology Books, 2014. ISBN: 9780080965321. URL: `https://books.google.at/books?id=tKPiQgAACAAJ`.

[7] M. Schmidt et al. "Lasers in Manufacturing 2011 - Proceedings of the Sixth International WLT Conference on Lasers in Manufacturing Utilisation of Thermal Radiation for Process Monitoring". In: *Physics Procedia* 12 (2011), pp. 704 –711. ISSN: 1875-3892. DOI: `http://dx.doi.org/10.1016/j.phpro.2011.03.088`. URL: `http://www.sciencedirect.com/science/article/pii/S1875389211001672`.

[8] R. Siegel. *Thermal Radiation Heat Transfer, Fourth Edition*. Thermal Radiation Heat Transfer. Taylor & Francis, 2001. ISBN: 9781560328391. URL: `https://books.google.at/books?id=O389yQ0-fecC`.

[9] Susan L. Blakeney, Sally E. Day, and J. Neil Stewart. "Determination of unknown input polarisation using a twisted nematic liquid crystal display with fixed components". In: *Optics Communications* 214.1–6 (2002), pp. 1 –8. ISSN: 0030-4018. DOI: `http://dx.doi.org/10.1016/S0030-4018(02)02115-6`. URL: `http://www.sciencedirect.com/science/article/pii/S0030401802021156`.

[10] Luc Gendre, Alban Foulonneau, and Laurent Bigué. "Imaging linear polarimetry using a single ferroelectric liquid crystal modulator". In: *Appl. Opt.* 49.25 (2010), pp. 4687–4699. DOI: `10.1364/AO.49.004687`. URL: `http://ao.osa.org/abstract.cfm?URI=ao-49-25-4687`.

[11] Władysław A. Woźniak, Marzena Prętka, and Piotr Kurzynowski. “Imaging Stokes polarimeter based on a single liquid crystal variable retarder”. In: *Appl. Opt.* 54.20 (2015), pp. 6177–6181. DOI: 10.1364/AO.54.006177. URL: http://ao.osa.org/abstract.cfm?URI=ao-54-20-6177.

[12] https://cdn.miniphysics.com/wp-content/uploads/2015/09/EM-Plane-Waves.png. Access date: 2016/10/22.

[13] D. Clarke and J.F. Grainger. *Polarized light and optical measurement.* International series of monographs in natural philosophy. Pergamon Press, 1971. URL: https://books.google.ie/books?id=agUvAAAAIAAJ.

[14] E. Hecht. *Optik.* Addison-Wesley, 1989. ISBN: 9783925118869. URL: https://books.google.at/books?id=lzCnSgAACAAJ.

[15] David S Kliger and James W Lewis. *Polarized light in optics and spectroscopy.* Elsevier, 2012.

[16] Georgiy V Tkachenko et al. *Nematic Liquid Crystal Confined in Electrochemically Etched Porous Silicon: Optical Characterization and Applications in Photonics.* INTECH Open Access Publisher, 2009.

[17] I.C. Khoo. *Liquid Crystals.* Wiley Series in Pure and Applied Optics. Wiley, 2007. ISBN: 9780471751533. URL: https://books.google.at/books?id=o0tRAAAAMAAJ.

[18] Alberto Sanchez-Castillo, Mikhail A. Osipov, and Frank Giesselmann. “Orientational order parameters in liquid crystals: A comparative study of x-ray diffraction and polarized Raman spectroscopy results”. In: *Phys. Rev. E* 81 (2 2010), p. 021707. DOI: 10.1103/PhysRevE.81.021707. URL: http://link.aps.org/doi/10.1103/PhysRevE.81.021707.

[19] Juan M Bueno. “Polarimetry using liquid-crystal variable retarders: theory and calibration”. In: *Journal of Optics A: Pure and Applied Optics* 2.3 (2000), p. 216. URL: http://stacks.iop.org/1464-4258/2/i=3/a=308.

[20] https://www.global-optosigma.com/en_us/images/category/opt_d/opt_d03_img11.jpg. Access date: 2016/10/22.

[21] Hans Neumann, Kurt Stecker, and Raimund Horch. *Temperaturmessung.* Akademie-Verlag, 1987.

[22] E.D. Palik. *Handbook of Optical Constants of Solids.* Academic Press handbook series vol. 3. Academic Press, 1998. ISBN: 9780125444231. URL: https://books.google.at/books?id=nxoqxyoHfbIC.

[23] https://www.thorlabs.de/images/large/TTN040104-lrg.jpg. Access date: 2016/10/22.

[24] https://www.thorlabs.de/images/TabImages/PBS_1200_G2-780.gif. Access date: 2016/10/22.

[25] https://www.thorlabs.de/images/large/23942-lrg.jpg. Access date: 2016/10/22.

[26] https://www.thorlabs.de/images/TabImages/LCC1xx1-C_Transmission_780.gif. Access date: 2016/10/22.

[27] https://www.thorlabs.de/images/large/TTN040010-lrg.jpg. Access date: 2016/10/22.

[28] https://www.hamamatsu.com/blobs/1328779674576?blobheadername1=content-disposition&blobheadervalue1=inline. Access date: 2016/10/22.

[29] dev.emcelettronica.com/files/u7555/Fig1.png. Access date: 2016/10/22.

[30] Thomas Pauger. "Diodenbasierte Prozessüberwachung eines Remote-Schneidprozesses basierend auf einer Polarisationsmessung". MA thesis. Adolf-Blamauer-Gasse 1-3 / Rella-Halle 1030 Wien: TUWien, Institut für Fertigungstechnik und Hochleistungslasertechnik, 2014.

[31] Kazuhiko Kobayashi and Moin Us Salam. "Comparing simulated and measured values using mean squared deviation and its components". In: *Agronomy Journal* 92.2 (2000), pp. 345–352.